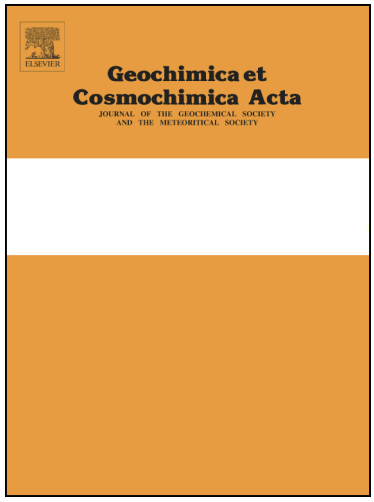

Hydrothermal sediments are a source of water column Fe and Mn in the Bransfield Strait, Antarctica

Alfred Aquilina, William B. Homoky, Jeffrey A. Hawkes, Timothy W. Lyons, Rachel A. Mills

PII: S0016-7037(14)00225-7
DOI: http://dx.doi.org/10.1016/j.gca.2014.04.003
Reference: GCA 8753

To appear in: *Geochimica et Cosmochimica Acta*

Received Date: 29 September 2013
Accepted Date: 2 April 2014

Please cite this article as: Aquilina, A., Homoky, W.B., Hawkes, J.A., Lyons, T.W., Mills, R.A., Hydrothermal sediments are a source of water column Fe and Mn in the Bransfield Strait, Antarctica, *Geochimica et Cosmochimica Acta* (2014), doi: http://dx.doi.org/10.1016/j.gca.2014.04.003

Hydrothermal sediments are a source of water column Fe and Mn in the Bransfield Strait, Antarctica

Alfred Aquilina[1], William B. Homoky[1,2], Jeffrey A. Hawkes[1,3], Timothy W. Lyons[4], Rachel A. Mills[1]

[1]Ocean and Earth Science, National Oceanography Centre Southampton, University of Southampton, Southampton, SO14 3ZH, United Kingdom

[2]Department of Earth Sciences, University of Oxford, South Parks Road, Oxford, OX1 3AN, United Kingdom

[3]Institute for Chemistry and Biology of the Marine Environment, University of Oldenburg, Oldenburg, Germany

[4]Department of Earth Sciences, University of California, Riverside, CA92521, USA

* Corresponding author: Rachel Mills (Email: Rachel.mills@soton.ac.uk)

ABSTRACT

Short sediment cores were collected from ~1100 m water depth at the top of Hook Ridge, a submarine volcanic edifice in the Central Basin of the Bransfield Strait, Antarctica, to assess Fe and Mn supply to the water column. Low-temperature hydrothermal fluids advect through these sediments and, in places, subsurface H_2S is present at high enough concentrations to support abundant *Sclerolinum* sp., an infaunal tubeworm that hosts symbiotic thiotrophic bacteria. The water column is fully oxic, and oxygen penetration depths at all sites are 2-5 cmbsf. Pore water Fe and Mn content is high within the subsurface ferruginous zone (max. 565 μmol Fe L^{-1}, >3 to 7 cmbsf)—14-18 times higher than values measured at a nearby, background site of equivalent water depth. Diffision and advection of pore waters supply significant Fe and Mn to the surface sediment. Sequential extraction of the sediment demonstrates that there is a significant enrichment in a suite of reactive, authigenic Fe minerals in the upper 0-5 cm of sediment at one site characterised by weathered crusts at the seafloor. At a site with only minor authigenic mineral surface enrichment we infer that leakage of pore water Fe and Mn from the sediment leads to enriched total dissolvable Fe and Mn in bottom waters. The largest Eh anomaly observed from our Bransfield Strait survey is associated with the elevated total dissolvable metal content in the

water column above this coring site.. We hypothesize that the main mechanism for Fe and Mn efflux from the sediment is breach of the surface oxic layer by the abundant *Sclerolinum* sp., along with episodic enhancements by physical mixing and resuspension of sediment in this dynamic volcanic environment. We propose that Hook Ridge sediments are an important source of Fe and Mn to the deep waters of the Central Basin in the Bransfield Strait, where concentrations are sustained by the benthic flux, and Fe is stabilised in the water column as either colloidal phases or ligand-bound dissolved species. Entrainment of this water mass into the Drake Passage and thereby the Antarctic Circumpolar Current could provide a significant metal source to this HNLC region of the Southern Ocean if mixing and upwelling occurs before removal of this metal pool to underlying sediments. Sediment-covered volcanic ridges are common within rifted margins and may play a previously overlooked role in the global Fe cycle.

1. INTRODUCTION

The surface waters of the Southern Ocean are generally characterized by low levels of primary productivity in spite of an abundant supply of macronutrients, but the distribution of phytoplankton biomass is highly variable, with some regions significantly more productive than others (Sullivan et al., 1993; Pollard et al., 2007). It is well established that the limited availability of Fe underpins restricted phytoplankton growth in the otherwise macronutrient-rich regions (high nutrient, low chlorophyll [HNLC]) of the Southern Ocean, thereby controlling the efficiency of the carbon pump (e.g., Martin et al., 1990; Blain et al., 2007; Hopkinson et al., 2007). The productivity varies seasonally, when conditions permit, around or downstream of islands, along the continental shelf and in the Antarctic Polar Frontal Zone (Sullivan et al., 1993). In particular, a marked gradient in surface primary productivity occurs across the southern Drake Passage where a region of low-chlorophyll waters, which extends across the eastern South Pacific sector of the Southern Ocean, gives way to high chlorophyll waters that extend across the Scotia Sea to the South Sandwich Islands (Sullivan et al., 1993; Ardelan et al., 2010). This productivity 'hot spot' is inferred to be sourced by Fe-replete waters originating in the South Shetland Island-Antarctic Peninsula region (Dulaiova et al., 2009), where Fe enrichment has been attributed to entrainment of inputs from diagenetically modified shelf sediments (Hatta et al., 2012; Measures et al., 2013).

The oxidation of organic matter in marine sediments can be redox-coupled to the reductive dissolution of manganese oxide and ferric minerals (Froelich et al., 1979) and can occur at rates sufficient to generate a flux of dissolved Mn (Heggie et al., 1987; Johnson et al., 1992; Slomp et al., 1997; McManus et al., 2012) and Fe (Berelson et al., 2003; Elrod et al., 2004; Pakhomova et al., 2007; Severmann et al., 2010; Homoky et al., 2012) to overlying waters. This benthic flux of Fe may vary by up to four orders of magnitude between shelf regions (Homoky et al., 2013), yet flux constraints from diverse ocean margin settings are very limited. The highest fluxes have been attributed to low oxygen bottom waters and high organic carbon oxidation rates (Severmann et al., 2010; Homoky et al., 2012; Noffke et al., 2012), while bio-irrigation of ferruginous sediments may enhance the efficacy of benthic exchange (Elrod et al., 2004; Severmann et al., 2010). There is additional evidence for high rates of Fe and Mn dissolution during the alteration of volcanic minerals (Homoky et al., 2011), which is suggested to result from inorganically driven mineral dissolution (Radic et al., 2011; Homoky et al., 2011; 2013). However the mechanisms, distribution and significance of these diagenetic settings are rarely examined, despite being a potentially important source of dissolved Fe and Mn to bottom waters across ocean basins.

High temperature vents have recently been recognised as an important source of particulate and bioavailable Fe to the deep ocean (Toner et al., 2012). There is now also mounting evidence that high-temperature vents are a major contributor to the dissolved Fe inventory of the deep ocean (e.g., Chu et al., 2006; Bennett et al., 2008; Tagliabue et al., 2010; Wu et al., 2011; Nishioka et al., 2013; Hawkes et al., 2013; Saito et al., 2013). Iron stabilisation and dispersion occurs through Fe-ligand complex and aggregate formation (Sander and Koschinsky, 2011; Hawkes et al., 2013) and the dispersion of pyrite nanoparticles over large distances in the deep ocean (Yücel et al., 2011). Modelling studies indicate the importance of hydrothermalism for dissolved Fe budgets in the Southern Ocean, where inclusion of hydrothermal inputs in the model is necessary to reproduce the observed water column Fe inventory (Tagliabue et al., 2014). Vent proximal hydrothermal sediments represent a hitherto unrecognized source of dissolved Fe in the world ocean.

The Bransfield Strait is a volcanically active marginal basin that is actively rifting the Antarctic Peninsula from the South Shetland Islands. Geologically recent volcanic activity in the region is recorded as geochemically distinct metalliferous layers in the sediments of the Central Basin (Fabrés et al., 2000; Fretzdorff and Smellie, 2002). Furthermore, submarine

volcanic edifices, such as Hook Ridge, in the Central Basin are hydrothermally active (Dählmann et al., 2001), producing a range of hydrothermal precipitates (Petersen et al., 2004) and elevated total and dissolved Fe and Mn in the water column (Klinkhammer et al., 2001). Sediments in the deeper basin comprise laminated siliceous oozes and massive siliceous muds with low carbonate content (<1 %) and relatively high organic carbon content (~1 %) (Yoon et al., 1994), whereas sediments on the volcanic edifices are influenced by local hydrothermal activity (Petersen et al., 2004).

This manuscript presents the results of a study designed to investigate the distribution of Fe and Mn in hydrothermal sediments and bottom waters over the Hook Ridge, a volcanic edifice located on the central rift axis at the eastern end of the central Bransfield Strait, which is covered by a layer of sediment to a depth of at least several metres. Low-temperature hydrothermal fluids advect through sediments at the top of Hook Ridge at rates up to 40 cm yr^{-1}, and abundant infaunal tube worms (*Sclerolinum* sp.) are observed at sites with sufficient H_2S supply to support chemosynthetic symbionts (Sahling et al., 2005; Aquilina et al., 2013). We demonstrate that biological breach of the surface oxic layer within metalliferous sediments from Hook Ridge is the most likely source of Fe and Mn to the metal-enriched bottom waters in the Central Basin of the Bransfield Strait and thus to the southern Drake Passage.

2. METHODS

2.1. Sediment and pore water sampling

Sediment samples were collected from the Central Basin of the Bransfield Strait during RRS James Cook expedition JC55 in January-February 2011 using a Bowers & Connelly Megacorer equipped with multiple polycarbonate core tubes (10 cm diameter). All necessary permits (numbers S5-4/2010) were obtained from the South Sandwich Islands Government, in accordance with the Antarctic Act 1994 and the Antarctic Regulations 1995. Sediment cores were collected from two adjacent stations (~1.3 km apart) near the top of Hook Ridge: cores MC7 and MC16 (previously described by Aquilina et al., 2013) at water depths of 1040 and 1174 m, respectively (Figure 1). Background cores (MC1, MC2 and MC3) were collected from a non-hydrothermally influenced station on the Antarctic Peninsula shelf, about 20 km south of the Hook Ridge stations at an equivalent water depth, to provide a control site for this study (Figure 1; Aquilina et al., 2013). Cores (23-36 cm

long) with an undisturbed sediment-seawater interface were immediately capped and transferred to a temperature-controlled laboratory (4°C) for further processing.

Shipboard determinations of dissolved oxygen content in the upper sediment were carried out on a dedicated core from each site as described by Homoky et al. (2011; 2013). A Unisense OX50 micro-sensor was calibrated between O_2-saturated and anoxic seawater solutions with temperature and salinity equivalent to bottom waters. Unisense micro-profiling apparatus and SensorTrace PRO software resolved oxygen content at 100 and 200 μm intervals down-core. Profiles penetrated the surface 1.6 to 3.9 cm of sediment cores but did not always reach the maximum penetration depth of oxygen due to restrictions of the sensor mounting. Oxygen profiles were later surface-normalised to bottom water values determined from CTD casts. High-resolution profiles are presented in Figure 2, and cm-averaged data are reported in data Table 2.

For pore water extraction, sediment cores were immediately transferred to a glove bag under oxygen-free N_2. The cores were manually extruded (at depth intervals of 1 or 2 cm) into a polycarbonate ring and sectioned using a PTFE sheet that was cleaned with deionised water (MilliQ, Millipore) between samples. Pore water was separated from the sediment matrix by centrifugation at 12,000 G at 4°C for 10 minutes under N_2; the supernatant fluids were filtered under N_2 through disposable 0.2 μm cellulose nitrate membrane syringe filters (Whatman, UK). Filtered pore waters were divided for nutrient, H_2S, and metal analyses. Cl^-, Br^-, H_2S, and NH_4^+ concentrations were determined on board, and subsamples were frozen at -20°C for subsequent nutrient analysis at the National Oceanography Centre Southampton (NOCS). Samples for dissolved metal analysis were acidified (pH <2) by adding 2 μl of concentrated HCl (UpA, Romil) per 1 ml of sample. Acidified pore water samples were stored refrigerated, and conjugate sediments were freeze dried on board and stored at room temperature pending analysis at the NOCS.

2.2. Solid phase analysis

Sub-samples (~ 100 mg) of the bulk, homogenised sediment were completely dissolved using a four stage digestion protocol: (1) aqua regia attack with reflux overnight at 90°C; (2) a combined hydrofluoric and perchloric acid attack (ratio of 2:1.5) where the

samples were refluxed at 150°C overnight and dried down at 170°C, increasing to 190°C on the observation of white fumes; (3) a perchloric acid attack with immediate dry down at 190°C; and (4) dissolution in 6M HCl at 60°C overnight. Samples were finally diluted in 0.6 M HCl for analysis. The acid digests were analysed for major and minor constituents, including Fe, Mn, Ti, Al and S by Inductively Coupled Plasma-Optical Emission Spectroscopy (ICP-OES). Calibration standards were matrix matched; we corrected for blank and instrument drift by including calibration blanks and multi-element standards for each batch of ten analyses. Certified sediment standards MAG-1 (United States Geological Survey) and GSMS-2 (Chinese Academy of Geological Sciences; Wang et al., 1998) were used to assess the accuracy of the method (Table 1).

Six sub-samples from core MC16 were treated using a sequential extraction scheme to assess the distribution of Fe among different authigenic mineral phases that are abundant at this site (Poulton and Canfield, 2005). According to this technique, iron bound to carbonates, adsorbed, or exchangeable (CAE) is extracted with Na acetate at pH 4.5 for 48 h at 50 °C (Fe_{CAE}). Iron present as crystalline oxides such as goethite and hematite is extracted with dithionite at pH 4.8 for 2 h at room temperature (Fe_{ox}), and Fe present as magnetite is extracted with oxalate at pH 3.2 for 6 h at room temperature (Fe_{mag}). Iron present as pyrite (Fe_{py}) was measured separately by a chromous chloride extraction, following the method of Canfield et al. (1986). The highly reactive iron pool (Fe_{HR}) is defined as $Fe_{CAE} + Fe_{ox} + Fe_{mag} + Fe_{py}$. The residual refractory Fe pool is estimated by difference between Fe_{HR} and the total Fe content.

2.3. Total and organic carbon analysis

The total carbon concentration was determined by coulometry from the CO_2 released upon total combustion of the sediment, and the inorganic carbon content was determined from the CO_2 released upon sample acidification. The organic carbon concentration was derived from the difference between the total carbon and inorganic carbon concentrations. Repeat analyses and comparison with certified standards indicates that the precision of this technique was ±0.1 wt. % (1SD).

2.4. Pore water analysis

Acidified pore water samples were analysed by ICP-OES for a number of elements

including Fe and Mn. Samples were diluted 50-fold in 0.6 M HCl, and concentrations were determined by external calibration against matrix-matched standard solutions. Instrument drift and blank were monitored and corrected for by measuring standard solutions and calibration blanks for every batch of ten analyses. Instrument limits of detection (3SD of blank) were 23 nM and 1.8 nM for Fe and Mn, respectively, corresponding to method detection limits of 1.1 μM and 0.09 μM for Fe and Mn, respectively. Accuracy was assessed by comparison to data generated by Inductively Coupled Plasma - Mass spectrometry (ICP-MS): Fe concentrations measured by ICP-OES were always within 10% of those measured by ICP-MS, and Mn concentrations were always within 5%. Due to the large sample requirements for ICP-OES, replicate pore water samples were not analysed.

Duplicate photometric nutrient analyses were made on samples which had been defrosted at 4^{o}C for 12 hours and 72 hours using an autoanalyser (QuAAtro; Seal Analytical). Data presented are for the 12 hour defrost period and data were excluded if the 72 hour defrost measurement was significantly lower (see Table 2). Instrument precision, determined from five replicate measurements of the same sample, was better than 2%, and measured concentrations of an artificial seawater standard (CRM-SW; High-Purity Standards) were within 1% of the recommended values. Hydrogen sulfide was fixed with zinc acetate and determined using standard photometric methods (Cline, 1969); the limit of detection (LOD) for this technique was ~1 M H_2S. Concentrations of Cl^- and SO_4^{2-} were determined at sea by ion chromatography (Dionex ICS2500), and the reproducibility for both was better than 2%, as determined by replicate analyses of samples and IAPSO standard seawater (Ocean Scientific International Ltd, UK).

2.5 Water column chemistry, TDFe and TDMn determination

Hydrothermal anomalies were detected using a Seabird +911 conductivity, temperature, and depth (CTD) profiler system that was equipped with a light scattering sensor (LSS) and a bespoke Eh detector (Nakamura et al., 2000). The Eh detector is sensitive to oxidation of nanomolar concentrations of reduced species on a platinum electrode, the potential of which is compared with an Ag/AgCl reference electrode in situ. Due to hysteresis and temperature/pH effects, the reading is not absolute, and so it is a sensitive detector of change in Eh rather than generating absolute values (Nakamura et al., 2000). Thus, all data are presented as the rate of change of Eh with time during tow yo CTD deployments (dEh/dt), and we only plot negative values where dEh/dt is decreasing for clarity. dEh/dt anomalies

indicate where fresh reduced species are being oxidised on the electrode. The CTD system was mounted on a titanium frame with 24 trace-metal-clean 10 litre OTE (Ocean Test Equipment) bottles, which were used to take seawater samples within the detected hydrothermal anomalies. Samples for total dissolvable metals (TDMn, TDFe) were collected after several rinses in 500 ml LDPE bottles that had been soaked in concentrated hydrochloric (1 week) and nitric (1 week) acid before being thoroughly rinsed with deionised water and stored in 0.1% sub-boiled nitric acid for bottle conditioning. The seawater samples were acidified to pH 1.9 with sub-boiled nitric acid (Optima, Fisher Scientific) and stored at room temperature for several months before analysis on shore. Metals were pre-concentrated from 100 ml of sample by mixed ligand extraction (Bruland et al., 1979) and dilution in 2% sub-boiled nitric acid. They were analysed using ICP-MS (Thermo Scientific X-series). Deionised water was used to determine the procedural blank (Mn = 0.08 nM, Fe = 0.62 nM), and the LOD (3σ of blank, n = 27) for Mn and Fe was 0.14 and 0.70 nM, respectively. Accuracy was assessed using certified seawater (NASS-5) and was within error of certified values (see Table 1).

3. RESULTS

3.1 Sediment composition and biogeochemical zonation

Sediments collected from Hook Ridge and the background site are homogenous siliceous muds that grade from brown at the surface through to grey at depth, and the total carbon content (mean 0.7 ± 0.2 wt. %, 0-35 cmbsf, *n* = 26) is almost entirely dominated by organic rather than inorganic carbon (Figure 2). There is a small surface enrichment in inorganic carbon at site MC16 and at the background site, which is a common feature of sediments in this region (Howe et al., 2007). No surface enrichment in inorganic carbon is seen at site MC7. The surface sediment at site MC16 is bright orange/red in colour, which is not observed at MC7. There is a distinct black layer near the base (33 cmbsf) of core MC7 that is inferred to be due to the presence of iron monosulfides (total S content = 1.2 wt% c.f. 0.2% through the rest of the core). The redox state, biogeochemical zonation, and upward advection of low-temperature hydrothermal fluids through these sediments have been described previously (Aquilina et al., 2013) and are summarised in Fig. 2. The hydrothermal fluids are inferred to be derived from phase separation of heated, modified seawater at depth

within the volcanic edifice which drives the observed advection through the sediments on Hook Ridge (Dahlmann et al., 2001).

The upper few cm of the sediment is oxic, and nitrate penetrates several cmbsf at each site. The oxygen penetration depth is inferred to be between 2-5 cm at each site based on oxygen microsensor deployments within retrieved cores on board ship and the pore water nitrate content (Fig. 2). The manganous and ferruginous zones extend through the remaining core depth, with some sulfate reduction at depth at all sites. There is a good correlation between SO_4^{2-} and Cl^- content in the pore waters collected across all sites (Fig. 3a). The main control on SO_4^{2-} content is seawater mixing with low chlorinity, low sulfate hydrothermal fluid, which is advecting upwards from beneath the sediment pile at rates of 9 cm yr^{-1} (MC7) and 33 cm yr^{-1} (MC16; Aquilina et al., 2013). Aquilina et al. (2013) estimated a hydrothermal end-member Cl^- content of 22 mM for these fluids and theoretical mixing for this fluid with seawater is shown in Fig. 3a. Some samples from each site exhibit SO_4^{2-} values that are lower than the mixing line, which is attributed to *in situ* sulfate reduction (Fig. 3a). Elevated H_2S (>10 cmbsf and up to 160 M at 30-32 cmbsf) is only observed at site MC7 (Fig. 2). H_2S levels at site MC16 are <6 M throughout the core, whereas H_2S is not detectable in the background core (Table 2).

An infaunal Annelid tubeworm, *Sclerolinum* sp.is abundant at site MC7; distributions of this species are controlled by the subseafloor supply of H_2S, and they are abundant in sediments where H_2S concentrations are ~150 M at 10-20 cmbsf (Sahling et al., 2005). *Sclerolinum* sp. were abundant in the upper 15 cm of the sediment at MC7 but is not observed at site MC16 or the background sites MC2 and MC3 (A. Glover, pers. comm. 2011).

3.2. Fe and Mn distributions in Hook Ridge sediments

The surface sediment on Hook Ridge site MC16 has a red-orange crust enriched in Fe and Mn, with high Fe/Ti and Mn/Ti ratios compared with recent volcanic material (Figure 2: Fe/Ti = 6.7-8.9 wt/wt and Mn/Ti = 0.1-0.17 wt/wt; Fretzdorff and Smellie, 2002), which is known to make up the majority of the lithogenic sediment component (Yoon et al., 1994). There is significant authigenic precipitation of Fe and Mn phases in the top ~5 cm at site MC16, seen as high Fe/Ti and Mn/Ti ratios in surface sediments, whereas surface authigenic

enrichment of Fe and Mn at site MC7 is not significantly different from the background site (Fig. 2). Site MC7 has small subsurface Fe and Mn maxima at ~10 and 5 cmbsf, respectively (Table 2).

3.2.1. Solid phase Fe speciation

The relative abundance of various operationally defined reactive Fe phases were determined in six samples to further investigate the response of Fe to early diagenesis and to determine the nature of the oxidised crust material at MC16 (Figure 4; Table 3). As outlined in section 2.2, the highly reactive Fe pool (Fe_{HR}) consists of the carbonate, adsorbed, and exchangeable Fe (CAE), as well as oxide, magnetite, and pyrite phases, and can be compared to the total Fe content (Fe_T) (Figure 4). Highly reactive Fe phases are enriched in the upper oxic layer relative to the deeper layers (Fe_{HR}/Fe_T >0.5 at 0-1 cm, compared to $Fe_{HR}/Fe_T \approx 0.1$ below ~8 cmbsf). In the shallowest sample at 0-1 cm, the highly reactive pool comprises carbonate-associated and adsorbed/exchangeable Fe likely dominated by amorphous Fe, exchangeable Fe phases ($Fe_{CAE}/Fe_{HR} \approx 0.4$), an easily reducible crystalline oxide ($Fe_{ox}/Fe_{HR} \approx 0.5$), and magnetite ($Fe_{mag}/Fe_{HR} \approx 0.1$). The pyrite content shows an overall increase with depth but is nonetheless low in all of the measured samples (Fe_{py} = 0.04 – 0.19 wt. %; $Fe_{py}/Fe_T < 0.03$), consistent with very low pore water H_2S content (<6 M) at this site (Figure 2; Aquilina et al., 2013). The residual Fe phase comprises unreactive lattice-bound Fe minerals and is relatively constant down core (~3.7 wt %; Table 3); this phase is inferred to be sourced from local volcanic inputs as observed in nearby basin sediments and ice rafted debris from the magmatic arc of the Bransfield Strait and the South Shetland Islands (Fretzdorff and Smellie, 2002).

3.2.2. Pore water Fe and Mn distributions

Cores from the hydrothermally influenced sites MC7 and MC16 have pore water Fe and Mn concentrations that are elevated to values 14-18 times higher than ferruginous pore waters in the background core, which are more typical of the deep shelf environment (up to 31 M; Figure 2). The lowest pore water Fe and Mn concentrations in the Hook Ridge cores occur in the shallowest layers close to the sediment-seawater interface, consistent with removal by oxidative precipitation in the surface oxygenated layer. Distinct sub-surface

dissolved Mn maxima (75-95 M) occur at 3-4 and 5-6 cm at sites MC16 and MC7, respectively, and broad subsurface Fe concentration maxima (100-500 M) occur between depth intervals of 3-17 cm and 6-24 cm at sites MC16 and MC7, respectively. Iron and manganese contents are independent of Cl content (Fig. 3b and c), with the highest pore water metal contents present at mid-depth in the Hook Ridge cores.

3.3.3 Water column Fe, Mn and Eh anomalies

Total dissolvable Fe (TDFe) and Mn (TDMn) contents were determined in bottom waters at depths of 10 to 113 m above the seafloor on Hook Ridge above the MC7 core site. Total dissolvable metals—determined on unfiltered, acidified water samples—comprise truly dissolved, ligand bound, colloidal, and suspended leachable particulate phases. TDFe and TDMn concentrations above Hook Ridge are significantly elevated (up to 41 nM and 5.1 nM, respectively; Table 4). These data match observations of widespread bottom water enrichment in TDFe and TDMn over the entire Hook Ridge by Klinkhammer et al. (2001), and their closest CTD cast is included for comparison in Table 4. These authors demonstrated, by comparison with the truly dissolved metal determinations, that the majority of the TDFe was present as suspended particulate, amorphous oxyhydroxide species, whereas the majority of the TDMn was dissolved, which is consistent with the oxidation kinetics and relative solubilities of these elements in oxygenated seawater (von Langen et al., 1997; Liu and Millero, 2002).

Typical Southern Ocean deep water values (outside the Bransfield Strait) for truly dissolved Fe and Mn are <1 nM (Middag et al., 2011), whereas total dissolvable metal values are always higher, and in the Bransfield Strait are ~1.7 nM Fe (Ardelan et al., 2010) and ~1 nM Mn. Deep water determinations of TDFe and truly dissolved Fe are not available at the background site but measurements made at equivalent depths (1070 m) SW of Deception Island (TDFe = 1.4 nM) and in deep water (2150 m) East of Bridgeman Island (1.86 nM) indicate that deep waters in the Central Bransfield Strait away from the Hook Ridge have typical low deep water values (Dulaiova et al., 2009).

The four CTD tow yo surveys we conducted over Hook Ridge revealed consistent Eh anomalies at water depths between 900 – 1200 m over the MC7 core site and measurable anomalies dispersed over 3 km along Hook Ridge in a northeast direction (Figure 5). No

anomalies were observed anywhere else in the Bransfield Strait other than in a localised area close to the seafloor on the Middle Sister volcanic edifice (Aquilina et al., 2013). No temperature or particle anomalies were observed during any of our surveys, and the only evidence of discrete venting of fluids is from video survey of a single 1-2 m high edifice with shimmering water close to the MC7 site (Aquilina et al., 2013). The paucity of evidence for hydrothermal flow is in contrast to surveys in the late 1990s, which revealed sediment temperatures of ~40^{o}C in retrieved cores collected in this region (Dählmann et al., 2001). Decadal scale variability in hydrothermalism is not uncommon in dynamic volcanic environments (Von Damm et al., 1995; Yücel and Luther, 2013).

4. DISCUSSION

Sediment accumulation rates are high throughout the Bransfield Central Basin because of high seasonal productivity and significant supply of silty hemipelagic material. Linear sediment accumulation rates as high as 1.48 mm yr^{-1} have been estimated in the deep basin north of Hook Ridge (Howe et al., 2007). The Bransfield Strait is volcanically active, and the Deception Island volcano has generated a series of volcanic ash layers in the sedimentary record of the Central Basin (Fretzdorff and Smellie, 2002). We suggest that the Fe and Mn enrichment within the Hook Ridge cores studied here is related to episodic volcanic activity on Hook Ridge and further afield in the Bransfield Strait, depositing reactive volcanic material with a composition similar to that observed in ash layers in nearby sediments (Fretzdorff and Smellie, 2002). These sources are likely to be augmented by localised input of mineralised polymetallic sulfide chimney material and pyrite-marcasite crusts, which have been observed at the Hook Ridge (Petersen et al., 2004). Organic carbon supply to the seafloor is also episodic due to the highly productive and short austral spring bloom at this latitude.

Hook Ridge sediments have been studied previously to characterise the nature of the low-temperature hydrothermal fluid flow in this region (Dählmann et al., 2001; Sahling et al., 2005; Aquilina et al., 2013). Low chlorinity fluid is known to upwell at rates of 9-33 cm yr^{-1} through Hook Ridge sediments (Aquilina et al., 2013). Temperature anomalies of a few tens of degrees were observed in the sediments in the 1990s (Dählmann et al., 2001), but no temperature anomalies were observed during our extensive 2011 survey (Aquilina et al., 2013). The hydrothermal fluid is depleted in chloride, which is attributed to phase separation

at depth. The fluid is also depleted in major salinity components including Mg, SO_4^{2-} and metals and is enriched in Si, NH_4^+, CH_4, B, Ba, Li, and Ca (Aquilina et al., 2013). Core MC16 has a more significant hydrothermal contribution with approximately 10% hydrothermal fluid at 20 cmbsf (Fig. 3a; Aquilina et al., 2013). Hydrothermal advection of low-temperature fluids, non-steady state redox cycling of metals in this dynamic environment, and faunal disturbance of surface sediments lead to significant fluxes of Fe and Mn to the overlying water column at the Hook Ridge as discussed below.

4.1. Solid phase Fe and Mn distributions

The Fe/Ti ratio and Mn/Ti ratio can be used to compare the sediment composition to the background detrital phases present in the Bransfield Strait and make comparisons of metal cycling at each site studied here (Figure 2). During early diagenesis, reactive Fe and Mn phases repeatedly pass through a cycle of reductive dissolution, upward transport of Fe^{2+} and Mn^{2+}, and subsequent oxidation and precipitation in the surface oxygenated layer; this process is occurring at all of the sites studied but only leads to significant authigenic enrichment at site MC16. Subsurface peaks in authigenic Fe and Mn in core MC7, identified by elevated Fe/Ti and Mn/Ti relative to the lithogenic component, are attributed to past input of reactive material and non-steady state sedimentary conditions.

Further insight into the response of Fe to early diagenesis is provided by the distribution of authigenic Fe phases in core MC16. Highly reactive Fe phases dominate the total Fe content in the surface oxygenated layer (oxygen penetration depth at MC16 ~5 cmbsf, $Fe_{HR}/Fe_T > 0.5$ at 0-1 cm). The surface enrichment in Fe_{ox} phases is consistent with the high Fe/Ti ratios observed at this site and indicates authigenic precipitation of Fe phases. Moreover, the high Fe_{CAE} values at the surface suggest that Fe precipitation occurs as a variety of amorphous and carbonate-bound phases in the upper sediment. The low pyrite content in this core is consistent with the detectable but low measured H_2S concentrations (<6 M), and the overall down core increase in Fe_{py} indicates some precipitation of FeS_2 at depth.

Magnetite forms under ferruginous conditions in marine sediments (Roh et al., 2003), and surface magnetite enrichment (Fe_{mag} = 0.61 wt% at 0.5 cm and 0.83 wt% at 2.5 cm) is consistent with active formation of magnetite at the onset of ferruginous conditions. The surface enrichment in residual Fe content relative to deeper in the core at MC16 (Fig. 4) is interpreted as an increased supply of material to the upper core leading to non-steady state

conditions and input of a pool of reactive Fe and Mn phases that undergo reductive dissolution and contribute to the subsurface pore water maxima.

4.2 Pore water Fe and Mn distributions

In the Hook Ridge and background site sediments, it is likely that bioturbation and bioirrigation resupply oxidants such as dissolved oxygen and nitrate down to a few centimetres depth. The water column conditions above Hook Ridge that ultimately determine the patterns of sediment diagenesis, such as surface primary productivity and organic carbon supply to the seafloor, are similar to the nearby background site. Therefore, we interpret the overall high pore water concentrations of Fe and Mn at Hook Ridge (relative to the background sites) as resulting from localized non-steady state input of reactive volcanic and hydrothermal mineral material to the sediment surface, followed by subsequent mineral dissolution, redox mobilization, transport, and authigenic mineral formation. The coincidence of the subsurface Mn and Fe pore water peaks with solid phase enrichments of these metals in core MC7 is consistent with intermittent input of reactive metal phases and subsequent remobilisation below the depth of oxygen penetration.

Dissolved Fe and Mn generated from dissimilatory reduction reactions will be transported upwards from the pore water maxima by a number of processes, including molecular diffusion along the concentration gradient and advection associated with upward migration of the low-temperature hydrothermal fluid. We cannot use classical diagenetic models to estimate Fe fluxes across the several cm-thick oxic surface sediment layer because we do not have any constraints on reaction or removal rates in this setting. If we consider only the kinetics of Fe(II) oxidation, then oxic surface sediment layers >2 cm thick are sufficient to trap significant diffusive Fe fluxes as authigenic oxyhydroxides (Homoky et al., 2012). However, we can estimate advective and diffusive fluxes within the sediment in the region directly below the oxic interface where Fe and Mn are inferred to be present as dissolved divalent species. This corresponds to consideration of the pore water Fe (5.5-9 cmbsf at MC7 and 2.5-5.5 cmbsf at MC16) and Mn (0.5-5.5 cmbsf at MC7 and 0.5-3.5 cmbsf at MC16) gradients in the upper sediment at each site (Table 2). The effective diffusion coefficient in seawater for Fe and Mn at 0^{o}C (D_{sw}) was estimated from the diffusion coefficient at infinite dilution at 0^{o}C corrected for the viscosity of seawater (Li and Gregory, 1974). The bulk sediment diffusion coefficient (D_s) was then calculated using Eq 1, which

corrects for sediment tortuosity estimated from porosity measurements at the relevant core depths (ϕ=0.8 for MC16 and 5.5-9 cmbsf in MC7, ϕ=0.8 for 0.5-5.5 cmbsf at MC7)

$$D_s = \frac{D_{sw}}{1 - \ln(\phi^2)}$$

Eq. 1

The calculated D_s values for Fe and Mn at each site are shown in Table 5. The diffusive flux (J) of Fe and Mn is calculated using Eq. 2.

$$J_i = -\phi \cdot D_s \cdot \frac{dC_i}{dz}$$

Eq. 2

Where dC_i/dz is the concentration gradient of the element of interest (i). Diffusive fluxes of Fe and Mn in cores MC7 and MC16 are shown in Table 5. The maximum upward advective fluxes can be estimated from the pore water advection rate (Table 5, from Aquilina et al., 2013) and the maximum Fe and Mn content (Table 2). These Fe and Mn fluxes are shown in Table 5. The Peclet number (Pe) is the ratio of the rate of advection of a pore water species to the rate of diffusion. Pe values for Fe and Mn in Hook Ridge sediments are shown in Table 5 and range from 0.43-0.71 at MC7 and 1.4-1.5 at MC16 demonstrating that advection marginally dominates Fe and Mn transport at MC16 while diffusion marginally dominates at MC7.

The calculated fluxes of Fe into the surface oxic layer are at the high end of the range seen to escape from continental shelves (Severmann et al., 2010; Noffke et al., 2012; Homoky et al., 2013), and demonstrate the potential for these sediments to generate and sustain a significant dissolved fluxes of Fe to the overlying water column if the continuity of surface oxic layer were breached. The fluxes calculated for Mn are high and are similar to those determined from volcanogenic sediments around Montserrat (Homoky et al., 2011). The kinetics of Mn oxidation in seawater are slow (Von Langen et al., 1997) and a component of this upward flux of dissolved Mn is likely to be transported to the overlying water column and contribute to the observed bottom water Mn enrichment (Klinkhammer et al., 2001).

4.3 Sedimentary Fe and Mn input to the water column

The CTD survey of the Hook Ridge demonstrates that there is no apparent buoyant plume of reducing compounds at this volcanic edifice (Figure 5), and the Eh anomalies occur close to the top of Hook Ridge near site MC7. This is most likely the result of low temperature (non-buoyant), inputs of reduced compounds. The Eh detector may be activated by any reduced compound that can be oxidised on the surface of the electrode, and at Hook Ridge this is likely to be nanomolar levels of H_2S, Mn^{2+} and Fe^{2+}.

The Fe/Mn ratios of dissolved and particulate pools in seawater can been used to identify the sources of these elements (Measures et al., 2012; Hawkes et al., 2014). We follow this approach to constrain the likely sources of Fe and Mn to bottom water above Hook Ridge. Bottom water Fe/Mn ratios of total dissolvable (TDFe /TDMn) pools range from 7 to 9 and fall within the range determined by Klinkhammer et al. (2001) closest to our sampling stations (TDFe /TDMn = 4 to 12; Table 4). The pore water Fe/Mn ratio varies widely down core, and ratios similar to those in the overlying water column are observed at the depth of maximum dissolved Fe concentration and in surface sediment at the MC7 site (Figure 6). The pore water Fe/Mn ratio decreases towards the sediment surface (except at the MC7 site) because the rates of Fe oxidation and concomitant authigenic mineralisation exceed Mn oxidation rates in this zone, and the ratio decreases below the ferruginous zone due to FeS and FeS_2 precipitation. Solid phase Fe/Mn ratios are much higher (Fe/Mn = 28 to 82; Figure 6). The coincidence of the TDFe/TDMn ratio of bottom water with that of the subsurface ferruginous pore water maximum is consistent with this being the source of total dissolvable metal to the bottom waters. Resuspension of sediments and associated upward mixing of fine grained particulate material, will produce a TDFe/TDMn pool with a very high Fe/Mn ratio, and inputs from Mn-rich pore fluids (low Fe/Mn) would have to be invoked to produce the observed Fe/Mn ratios over the Hook Ridge.

Hook Ridge sediments host abundant *Sclerolinum* sp. (up to 800 individuals m^{-2}) in areas of measurable sulfide flux (Sahling et al., 2005). This small infaunal annelid worm inhabits tubes 0.2-0.4 mm in diameter with a maximum length of 15 cm (Sahling et al., 2005). The adult species is inferred to host obligate sulfide oxidising symbionts within the trophosome (Hilario et al., 2011), and thus the species distribution is controlled by sulfide supply within the upper sediment layers (Sahling et al., 2005). *Sclerolinum* sp. are abundant

at site MC7 where H_2S levels exceed 150 M and there is active advection of hydrothermal fluid through the sediment pile (Aquilina et al., 2013). These infaunal worms have no gut, mouth, or anus (Hilario et al., 2011), and when alive the symbionts actively uptake the sulfide present in the reduced fluids. On death the worm tube will provide a conduit for the upwardly advecting fluids present in this region (Sahling et al., 2005; Aquilina et al., 2013). We hypothesise that a significant flux of reduced Fe(II) and Mn(II) can bypass surface reaction and enter bottom waters directly via *Sclerolinum* sp. breach of the surface oxic layer at sites with abundant infaunal worm populations—leading to the observed enrichment in TDFe and TDMn in this region (Figure 5). The advection dominated pore water hydrology demonstrated by the Pe numbers close to unity suggest significant fluxes of Fe and Mn are possible. Our conceptual model of bioirrigation at this site is summarised in Figure 7. We propose that the abundant *Sclerolinum* sp. observed at site MC7 can lead to breach of the surface oxic layer and efflux to the overlying water (Figure 7). The main evidence for effective bypass of the surface sediment at site MC7 is the absence of any authigenic mineralisation at the sediment surface at this site (Fig. 2), the maximum in dEh/dt anomaly in the water directly overlying the sediment at this coring site (Figure 5), and the coincidence in Fe/Mn ratio between the pore water pool and the water column TDmetal pool (Fig. 6). In the absence of any breach of the surface oxic layer by infaunal *Sclerolinum* sp., the dissolved Fe and a proportion of the Mn precipitates in the surface zone as authigenic minerals (Figure 4). This process is inferred to dominate at site MC16, where significant surface authigenic mineral enrichments are observed.

Additionally, the Fe and Mn flux across the sediment-seawater interface can be augmented by sediment disturbance and resuspension processes, which would contribute by adding particle loading and releasing Fe- and Mn-enriched pore water to the benthic boundary layer. Indeed, resuspension of sediments is widely considered an important mechanism for Fe and Mn surface water enrichment above the shelf of the South Shetland Islands (e.g., Hatta et al., 2012; de Jong et al., 2012; Frants et al., 2013; Measures et al., 2013). On the shallower shelf region, resuspension is affected by the high velocity bottom currents interacting with shelf bathymetry; in this deeper environment, resuspension is more likely driven by volcanic activity and associated slumping, turbidite inputs, and disturbance to seafloor sediments—and will occur less frequently.

Bottom water enrichments in TDFe and TDMn are likely to remain in the water column because enhanced mixing occurs within the benthic boundary layer up to 100 m above the seafloor (typical K_v = 1 x10^9 m^2 s^{-1}; Chung and Kim, 1980), thus countering the theoretical settling velocity of nano-scale minerals in ocean water (~5 x10^{-8} m s^{-1}; Yücel et al., 2011). We suggest the wide-scale Eh anomaly above site MC7 (Fig. 5) and widespread total dissolvable metal enrichment reported by Klinkhammer et al. (2001) results from a sediment-enhanced total dissolvable metal inventory, which is mixed through the deep Bransfield Strait. Likely mechanisms to stabilise this hydrothermal Fe include retardation of oxidation kinetics (Hawkes et al., 2013), formation of pyrite nanoparticles (Yücel et al., 2011) and organic complexation (Sander and Koschinsky, 2011).

Net flow in the upper Bransfield Strait is towards the northeast, parallel to the shelf slope, and the surface mixed layer is as deep as 500 m in the austral winter (Zhou et al., 2013). The deep Central Basin waters are ventilated from the Weddell Sea and transported out of the Strait along the northeast shelf slope (Gordon et al., 2000). Water that exits into the Drake Passage entrains water from the Bransfield Strait shelf slope and deeper Central Basin water that has acquired elevated TDFe and TDMn from Hook Ridge (Zhou et al., 2013). Thus, this source potentially fuels primary production in the Southern Ocean as this deep water mass is mixed upwards into the surface mixed layer and is made available for biological uptake (Tagliabue et al., 2010).

5. CONCLUSIONS

Intermittent input of reactive volcanic and hydrothermal material to Hook Ridge sediments leads to non-steady state conditions in Fe and Mn supply and reaction compared with background shelf sediments. Sub-seafloor pore water Fe and Mn content is extremely high compared to that measured at the background shelf site because of enhanced dissolution from the reactive volcanic and hydrothermal phases.

Fluxes to the surface sediment occur via molecular diffusion augmented by the net upward advection of the subsurface Fe and Mn maxima at this site (Peclet numbers range from 0.4 to 1.5), and authigenic mineralisation occurs unless there is a breach of the surface layer. The surface authigenic mineral assemblage is characteristic of Fe-rich crusts and deposits commonly associated with seafloor volcanism and continental rifting.

One mechanism for breaching the oxide trap is the infaunal lifestyle of the abundant *Sclerolinum* sp. in areas of ample H_2S supply, such as site MC7. Mapped water column dEh/dt distributions show that there are no buoyant seafloor venting features in this region. Instead, the Eh distribution suggests a bathymetry-hugging effluent, which is most likely sourced from sediments from the top of Hook Ridge. Our analyses, building on previous work, demonstrate that worm abundance is a function of H_2S supply to surface sediment and that there is a specialised community of *Sclerolinum* sp. worms at Hook Ridge inhabiting this low-temperature environment. We infer that breach of the surface oxidised layer of these hydrothermal sediments leads to a significant flux of TDFe and TDMn from the subseafloor ferruginous and manganous zones into the lower water column. This input leads to significantly elevated TDFe and TDMn over the Hook Ridge, which will be dispersed through the Bransfield Strait and mixed into the Drake Passage, thereby supplying these metals to the upper mixed layer and associated phytoplankton communities (Frants et al., 2013). Sediment-hosted rifted margins are relatively common but have been overlooked as a source of dissolved Fe and Mn to the oceans.

ACKNOWLEDGEMENTS

The authors would like to thank the officers, technicians and crew aboard the RRS *James Cook* for supporting the sampling in the Bransfield Strait, and the staff of the UK National Marine Facilities at NOC for logistic and shipboard support. We thank Ko-ichi Nakamura from the National Institute of Advanced Industrial Science and Technology, Tsukuba, Japan for the loan of the Eh sensor for this work. Laura Hepburn and Darryl Green provided invaluable analytical support at sea and in the laboratory. Veerle Huvenne and Leigh Marsh generated Figure 1. This expedition was funded by the NERC ChEsSo consortium (NERC Grant NE/DO1249X/1). TWL received support from the U.S. National Science Foundation.

FIGURE CAPTIONS

Figure 1. Regional map of the Antarctic Peninsula and Bransfield Strait (inset) and detailed bathymetry of the Central Basin within the Bransfield Strait showing coring sites

MC16 and MC7 on Hook Ridge and the background core site (MC1/MC2/MC3) on the Antarctic Peninsula shelf. All coring sites are at a depth of ~1100 m water depth. This map is constructed using GEBCO bathymetry.

Figure 2. Down-core schematic representation of biogeochemical zonation and the distribution of pore water and solid phase sediment compositions for (a) Hook Ridge site MC16, (b) Hook Ridge site MC7 and (c) the background shelf site MC1/2/3. The biogeochemical zonation is determined from pore water distributions of terminal electron acceptors (O_2, NO_3^-, Mn^{2+}, Fe^{2+} and H_2S) and previously published description of advection of hydrothermal fluids through the sediment (Aquilina et al., 2013). Oxygen microsensor data are plotted at 100 m depth intervals. Shaded area in Mn/Ti and Fe/Ti plots is the range of values for ash layers in Bransfield Strait sediments (Fretzdorff and Smellie, 2002).

Figure 3. Plots of (a) pore water SO_4^{2-} against Cl^- content for all cores, (b) pore water Mn content against Cl^- content and (c) pore water Fe content against Cl^- content. The dashed line in (a) shows the composition of mixtures of seawater with the inferred low salinity hydrothermal end member advecting through Hook Ridge sediments (Aquilina et al., 2013).

Figure 4. Solid-phase Fe distribution in Hook Ridge (site MC16) sediments. Highly reactive Fe (Fe_{HR}) is defined as the sum of Fe present as carbonate (Fe_{CAE}), oxide (Fe_{ox}), magnetite (Fe_{mag}) and pyrite (Fe_{py}), following determination by the sequential extraction of Poulton and Canfield (2005) and the pyrite determination technique of Canfield et al. (1986). Residual Fe is calculated from the difference between total Fe determinations and the sum of the highly reactive Fe species.

Figure 5. Profiles of total dissolvable metal content and reductive potential (Eh) over Hook Ridge. (a) Total dissolvable iron (TDFe) and manganese (TDMn) at four depths at stations CTD192 (solid circles) and CTD420 (open circle) (stations marked in B), with typical background concentrations shown as dashed lines. (b) Four sections of dEh/dt (change in reductive potential in mV/s) over Hook Ridge. Warmer colours show more negative reductive potential and therefore higher concentrations of electron donor species such as Fe^{2+} or H_2S. All positive values (i.e. where the detector is returning to background reading) are shown as zero for clarity. Coring sites MC7, MC16 and the two CTD profile stations are marked on the relevant sections.

Figure 6: Down core Fe/Mn molar ratios for pore fluid (closed symbols) and solid phase (open symbols) in Hook Ridge cores (MC7 and MC16). Water column Fe/Mn ratios are shown for comparison along with the range of data measured in the Hook Ridge vicinity for previous studies (Station 39, Klinkhammer et al., 2001).

Figure 7. Conceptual cartoon summarising the principal mechanisms for Fe reaction, transport and efflux from sediments on the Hook Ridge. The presence of significant *Sclerolinum* sp. is inferred to enhance transport of pore waters through the oxic layer into bottom waters and thus lead to the observed enrichment of total dissolvable Fe and Mn.

REFERENCES

Aquilina, A., Connelly, D. P., Copley, J. T., Green, D. R. H., Hawkes, J. A., Hepburn, L. E., Huvenne, V. A. I., Marsh, L., Mills, R. A. and Tyler, P. A. (2013) Geochemical and visual indicators of hydrothermal fluid flow through a sediment-hosted volcanic ridge in the Central Bransfield Basin (Antarctica). *PLoS ONE* **8,** e54686. doi:10.1371/journal.pone.0054686.

Ardelan, M. V., Holm-Hansen, O., Hewes, C. D., Reiss, C. S., Silva, N. S., Dulaiova, H., Steinnes, E. and Sakshaug, E. (2010) Natural iron enrichment around the Antarctic Peninsula in the Southern Ocean. *Biogeosciences* **7**, 11-25.

Bennett, S. A., Achterberg, E. P., Connelly, D. P., Statham, P. J., Fones, G. R. and German, C. R. (2008) The distribution and stabilisation of dissolved Fe in deep-sea hydrothermal plumes. *Earth Planet. Sci. Lett.* **270**, 157-167.

Berelson, W. M., McManus, J., Coale, K. H., Johnson, K. S., Burdige, D., Kilgore, T., Colodner, D., Chavez, F., Kudela, R. and Boucher, J. (2003) A time series of benthic flux measurements from Monterey Bay, CA. *Cont. Shelf Res.* **23**, 457.

Blain, S., Quéguiner, B., Armand, L., Belviso, S., Bombled, B., Bopp, L., Bowie, A., Brunet, C., Brussaard, C., Carlotti, F., Christaki, U., Corbiere, A., Durand, I., Ebersbach, F., Fuda, J.-L., Garcia, N., Gerringa, L., Griffiths, B., Guigue, C., Guillerm, C., Jacquet, S., Jeandel, C., Laan, P., Lefevre, D., Lo Monaco, C., Malits, A., Mosseri, J., Obernosterer, I., Park, Y.-H., Picheral, M., Pondaven, P., Remenyi, T., Sandroni, V., Sarthou, G., Savoye, N., Scouarnec, L., Souhaut, M., Thuiller, D., Timmermans, K., Trull, T., Uitz, J., van Beek, P., Veldhuis, M., Vincent, D., Viollier, E., Vong, L. and Wagener, T. (2007) Effect of natural iron fertilization on carbon sequestration in the Southern Ocean. *Nature* **446**, 1070-1075.

Bruland, K. W., Franks, R. P., Knauer, G. A. and Martin, J. H. (1979) Sampling and analytical methods for the determination of copper, cadmium, zinc and nickel at the nanogram per liter level in sea-water. *Anal. Chim. Acta* **105**, 233-245.

Canfield, D. E., Raiswell, R., Westrich, J. T., Reaves, C. M. and Berner, R. A. (1986) The use of chromium reduction in the analysis of reduced inorganic sulfur in sediments and shales. *Chem. Geol.* **54**, 149-155.

Chu, N.-C., Johnson, C. M., Beard, B. L., German, C. R., Nesbitt, R. W., Frank, M., Bohn, M., Kubik, P. W., Usui, A. and Graham, I. (2006) Evidence for hydrothermal venting in Fe isotope compositions of the deep Pacific Ocean through time. *Earth Planet. Sci. Lett.* **245**, 202-217.

Chung, Y. and Kim, K. (1980) Excess ^{222}Rn and the benthic boundary layer in the western and southern Indian Ocean. Earth *Planet. Sci. Lett.* **49**, 351-359.

Cline, J. D. (1969) Spectrophotometric determination of hydrogen sulfide in natural waters. *Limnol. Oceanogr*. **14**, 454–458.

Dählmann A, Wallmann K, Sahling H, Sarthou G, Bohrmann G, Petersen, S. Chin, C.S. and Klinkhammer, G.P. (2001) Hot vents in an ice-cold ocean: Indications for phase separation at the southernmost area of hydrothermal activity, Bransfield Strait, Antarctica. *Earth Planet. Sci. Lett.* **193**, 381–394.

De Jong, J., Schoemann, V., Lannuzel, D., Croot, P., de Baar, H. and Tison, J. L. (2012) Natural iron fertilization of the Atlantic sector of the Southern Ocean by continental shelf sources of the Antarctic Peninsula. *J. Geophys. Res: Biogeosciences*, **117**, G01029.

Dulaiova, H., Ardelan, M. V., Handerson, P. B., and Charette, M. A., 2009. Shelf-derived iron inputs drive biogeochemical productivity in the southern Drake Passage. *Glob. Biogeochem. Cycles* **23**, GB4014. doi: 10.1029/2008GB003406

Elrod, V. A., Berelson, W. M., Coale, K. H. and Johnson, K. S. (2004) The flux of iron from continental shelf sediments. *Geophys. Res. Lett.* **31**, L12307. doi:10.1029/2004GL020216.

Fabrés, J., Calafat, A., Canals, M., Bárcena, M. A. and Flores, J. A. (2000) Bransfield Basin fine-grained sediments: late-Holocene sedimentary processes and Antarctic oceanographic conditions. *The Holocene* **10,** 703-718.

Frants, M., Gille, S. T., Hatta, M., Hiscock, W. T., Kahru, M., Measures, C. I., Mitchell, B. G., and Zhou, M. (2013) Analysis of horizontal and vertical processes contributing to natural iron supply in the mixed layer in southern Drake Passage. *Deep Sea Res. II*, **90**, 68–76.

Fretzdorff, S. and Smellie, J. L. (2002) Electron microprobe characterization of ash layers in sediments from the central Bransfield basin (Antarctic Peninsula): evidence for at least two volcanic sources. *Antarct Sci* **14**, 412-421.

Froelich, P. N., Klinkhammer, G. P., Bender, M. L., Luedtke, N. A., Heath, G. R., Cullen, D., Dauphin, P., Hammond, D., Hartman, B. and Maynard, V. (1979) Early oxidation of organic matter in pelagic sediments of the eastern equatorial Atlantic: suboxic diagenesis. *Geochim. Cosmochim. Acta* **43**, 1075-1090.

Gordon, A. L., Mensch, M., Dong, Z., Smethie Jr, W. M. and de Bettencourt, J. (2000) Deep and bottom water of the Branfield Strait eastern and central basins. *J. Geophys. Res*. **105**, 11337-11346.

Hatta, M., Measures, C. I., Selph, K. E., Zhou, M. and Hiscock, W. T. (2012) Iron fluxes from the shelf regions near the South Shetland Islands in the Drake Passage during the austral-winter 2006. *Deep-Sea Res. II* **90**, 89-101.

Hawkes, J. A., Gledhill, M., Connelly, D. P. and Achterberg, E. P. (2013) The stabilisation and transportation of dissolved iron from high temperature hydrothermal vent systems. *Earth Planet. Sci. Lett*. **375**, 280-290.

Hawkes, J. A., D. P. Connelly, M. J. A. Rijkenberg, and E. P. Achterberg (2014), The importance of shallow hydrothermal island arc systems in ocean biogeochemistry, *Geophys. Res. Lett.,* **41**, doi:10.1002/2013GL058817

Heggie, D., Klinkhammer, G. and Cullen, D. (1987) Manganese and copper fluxes from continental margin sediments. *Geochim. Cosmochim. Acta* **51**, 1059–1070.

Hilario, A., Capa, M., Dahlgren, T. G., Halanych, K. M., Little, C. T. S., Thornhill, D. J., Verna, C. and Glover, A. G. (2011) New perspectives on the ecology and evolution of Siboglinid tubeworms. *PLoS ONE* **6,** e16309. doi:10.1371/journal.pone.0016309.

Homoky, W. B., Hembury, D. J., Hepburn, L. E., Mills, R. A., Statham P.J., Fones, G. and Palmer, M., (2011) Iron and manganese diagenesis in deep sea volcanogenic sediments and the origins of pore water colloids. *Geochim. Cosmochim. Acta* **75**, 5032-5048.

Homoky, W. B., John, S. G., Conway. T. M. and Mills, R. A. (2013) Distinct iron isotopic signatures and supply from marine sediment dissolution. *Nat. Commun*. **4**:2143 doi: 10.1038/ncomms3143

Homoky, W. B., Severmann, S., McManus, J., Berelson, W. M., Riedel, T. E., Statham, P.J. and Mills, R. A. (2012) Dissolved oxygen and suspended particles regulate the benthic flux of iron from continental margins. *Mar. Chem*. **134-135**, 59-70.

Hopkinson, B.M., G. Mitchell, R. Reynolds, H. Wang, C. Hewes, C. Measures, O. Holm-Hansen, and K.A. Barbeau. (2007) Iron limitation across chlorophyll gradients in the southern Drake Passage: phytoplankton responses to iron addition and indicators of iron stress. *Limnol. Oceanogr.* 52: 2540-2554.

Howe, J. A., Wilson, C. R., Shimmield, T. M., Diaz, R. J. and Carpenter, L. W. (2007) Recent deep-water sedimentation, trace metal and radioisotope geochemistry across the Southern Ocean and Northern Weddell Sea, Antarctica. *Deep-Sea Res. II* **54**, 1652-1681.

Johnson, K.S., Berelson,W.M., Coale, K.H., Coley, T.L., Elrod,V.A., Fairey,W.R., Iams,H.D., Kilgore, T.E. and Nowicki, J.L., (1992) Manganese flux from continental margin sediments in a transect through the oxygen minimum. *Science* **257**, 1242–1245.

Klinkhammer, G. P., Chin, C. S., Keller, R. A., Dählmann, A., Sahling, H., Sarthou, G., Petersen, S., Smith, F. and Wilson, C. (2001). Discovery of new hydrothermal vent sites in Bransfield Strait, Antarctica. *Earth Planet. Sci. Lett.* **193**, 395-407.

Li, Y.-H., and Gregory, S. (1974) Diffusion of ions in sea water and in deep-sea sediments. *Geochim. Cosmochim. Acta* **38**, 703-714.

Liu, X., and Millero, F. J. (2002) The solubility of iron in seawater. *Mar. Chem*. **77**, 43-54.

McManus, J., Berelson, W. M., Severmann, S., Johnson, K. S., Hammond, D. E., Roy, M., and Coale, K. H. (2012) Benthic manganese fluxes along the Oregon and California continental shelf and slope. *Cont. Shelf Res.* **43**, 71-85.

Martin, J. H., Fitzwater, S. E. and Gordon, R.M. (1990) Iron deficiency limits phytoplankton growth in Antarctic waters. *Glob. Biogeochem. Cycles* **4**, 5-12.

Measures, C. I., Hatta, M., and Grand, M. M. (2012) Bioactive trace metal distributions and biogeochemical controls in the Southern Ocean. *Oceanography* **25**, 122-133.

Measures, C. I., Brown, M.T., Selph, K.E., April, A., Zhou, M., Hatta, M., and Hiscock, M.V. (2013) The influence of shelf processes in delivering dissolved iron to the HNLC waters of the Drake Passage Antarctica. *Deep-Sea Res. II*, **90**, 77–88

Middag, R., De Baar, H. J. W., Laan, P., Cai, P. H., & Van Ooijen, J. C. (2011). Dissolved manganese in the Atlantic sector of the Southern Ocean. *Deep Sea Res. Part II*, *58*, 2661-2677.

Nakamura, K., Veirs, S., Sarason, C. P., McDuff, R. E., Stahr, F., Yoerger, D. R. and Bradley A. M. (2000) Chemical signals in rising buoyant plumes and tidally oscillating plumes at the Main Endeavour vent field, Juan de Fuca Ridge. *EOS Transactions—American Geophysical Union,* **81** OS52I-05.

Nishioka, J., Obata, H. and Tsumune, D. (2013) Evidence of an extensive spread of hydrothermal dissolved iron in the Indian Ocean. *Earth Planet. Sci. Letter.* **361**, 26-33.

Noffke, A., Hensen, C., Sommer, S., Scholz, F., Bohlen, L., Mosch, T., Graco, M. and Wallmann, K. (2012) Benthic iron and phosphorus fluxes across the Peruvian oxygen minimum zone. *Limnol. Oceanogr.* **57**, 851-867.

Pakhomova, S. V., Hall, P. O. J., Kononets, M. Y., Rozanov, A. G., Tengberg, A. and Vershinin, A. V. (2007) Fluxes of iron and manganese across the sediment-water interface under various redox conditions. *Mar. Chem.* **107**, 319-331.

Petersen, S., Herzig, P. M., Schwarz-Schampera, U., Hannington, M. D. and Jonasson, I. R. (2004) Hydrothermal precipitates associated with bimodal volcanism in the Central Bransfield Strait, Antarctica. *Miner. Deposita* **39**, 358-379.

Pollard, R. T., Venables, H. J., Read, J. F. and Allen, J. T. (2007) Large-scale circulation around the Crozet Plateau controls an annual phytoplankton bloom in the Crozet Basin. *Deep-Sea Res. II* **54**, 1915-1929.

Poulton, S. W. and Canfield, D. E. (2005) Development of a sequential extraction procedure for iron: implications for iron partitioning in continentally derived particulates. *Chem. Geol.* **214**, 209-221.

Radic, A., Lacan, F. and Murry, J. W. (2011) Iron isotopes in the seawater of the equatorial Pacific Ocean: New constraints for the oceanic iron cycle. *Earth Planet. Sci. Lett.* **306**, 1-10.

Roh, Y., Zhang, C. L., Vall, H., Lauf, R. J., Zhou, J. and Phelps, T. J. (2003) Biogeochemical and environmental factors in Fe biomineralization: Magnetite and siderite formation. *Clays Clay Miner.* **51**, 83-95.

Sahling, H., Wallmann, K., Dählmann, A., Schmaljohann, R. and Petersen, S. (2005) The physicochemical habitat of *Sclerolinum* sp.at Hook Ridge hydrothermal vent, Bransfield Strait, Antarctica. *Limnol. Oceanogr.* **50**, 598-606.

Saito, M. A., Noble, A. E., Tagliabue, A., Goepfert, T. J., Lamborg, C. H. and Jenkins, W. J. (2013) Slow-spreading submarine ridges in the South Atlantic as a significant oceanic iron source. Nature Geoscience, doi: 10.1038/NGEO1893.

Sander, S. G. and Koschinsky, A. (2011) Metal flux from hydrothermal vents increased by organic complexation. *Nat. Geosci.* **4**, 145-150.

Severmann, S., McManus, J., Berelson, W. M. and Hammond, D. E. (2010) The continental shelf benthic iron flux and its isotope composition. *Geochim. Cosmochim. Acta* **74**, 3984-4004.

Slomp, C.P., Malschaert, J.F.P., Lohse, L. and Van Raaphorst, W. (1997). Iron and manganese cycling in different sedimentary environments on the North Sea continental margin. *Cont. Shelf Res.* **17**, 1083–1117.

Sullivan, C. W., Arrigo, K. R., McClain, C. R., Comiso, J. C. and Firestone, J. (1993) Distributions of phytoplankton blooms in the Southern Ocean. *Science* **262**, 1832-1837.

Tagliabue, A., Bopp, L., Dutay, J.-C., Bowie, A. R., Chever, F., Jean-Baptiste, P., Bucciarelli, E., Lannuzel, D., Remenyi, T., Sarthou, G., Aumont, O., Gehlen, M. and Jeandel, C. (2010) Hydrothermal contribution to the oceanic dissolved iron inventory. *Nat. Geosci.* **3**, 252-256.

Tagliabue, A., Aumont, O. and Bopp, L. (2014) The impact of different external sources of iron on the global carbon cycle. Geophys. Res. Lett. 42, doi:10.1002/2013GL059059.

Toner, B. M., Macus, M. A., Edwards, K. J., Rouxel, O. and German, C. R. (2012) Measuring the form of iron in hydrothermal plume particles. *Oceanography* **25**, 209-212.

Von Damm, K. L., S. E. Oosting, R. Kozlowski, L. G. Buttermore, D. C. Colodner, H. N. Edmonds, J. M. Edmond, and J. M. Grebmeier (1995), Evolution of East Pacific Rise hydrothermal vent fluids following a volcanic eruption, *Nature*, **375**, 47–50, doi:10.1038/375047a0.

Von Langen, P. J., Johnson, K. S., Coale, K. H. and Elrod, V. A. (1997). Oxidation kinetics of manganese (II) in seawater at nanomolar concentrations. *Geochim. Cosmochim. Acta*, **61,** 4945-4954.

Wang, Y., Luo, D., Gao, Y., Song, H., Li, J., Chen, W., Teng, Y. and Zhou, S. (1998) A preliminary study on the preparation of four Pacific Ocean polymetallic nodule and sediment reference materials: GSPN-2, GSPN-3, GSMS-2 and GSMS-3. *Geostandard Newslett.* **22**, 247-254.

Wu, J., Wells, M. L. and Rember, R. (2011) Dissolved iron anomaly in the deep tropical-subtropical Pacific: Evidence for long-range transport of hydrothermal iron. *Geochim. Cosmochim. Acta* **75**, 460-468.

Yoon, H. I., Han, M. W., Park, B. K., Oh, J. K and Chang, S. K. (1994) Depositional environment of near-surface sediments, King George Basin, Bransfield Strait, Antarctica. *Geo-Mar. Lett.* **14**, 1-9.

Yücel, M., Gartman, A., Chan, C. S. and Luther, G. W., III (2011) Hydrothermal vents as a kinetically stable source of iron-sulfide-bearing nanoparticles to the ocean. *Nat. Geosci*. **4**, 367-371.

Yücel M. and Luther G. W. III (2013), Temporal trends in vent fluid iron and sulfide chemistry following the 2005/ 2006 eruption at East Pacific Rise, 9°50'N, *Geochem. Geophys. Geosyst*. **14**, 759–765, doi:10.1002/ggge.20088.

Zhou, M., Zhu, Y., Measures, C. I., Hatta, M., Charette, M. A., Gille, S. T., Frants, M., Jiang, M. and Mitchell, B. G. (2013) Winter mesoscale circulation on the shelf slope region of the southern Drake Passage. *Deep Sea Res. II* **90,** 4-14.

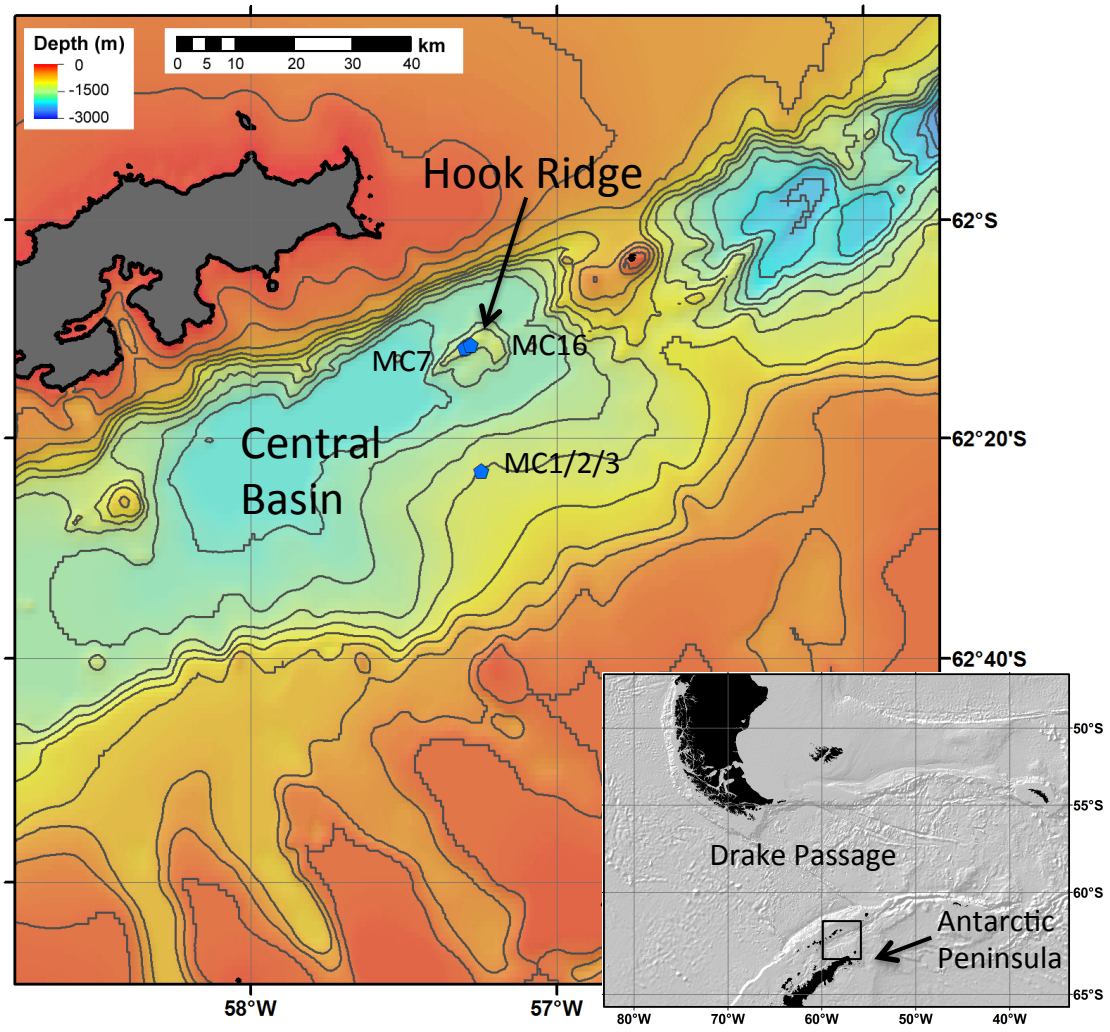

Aquilina et al., Figure 1

(a) MC16

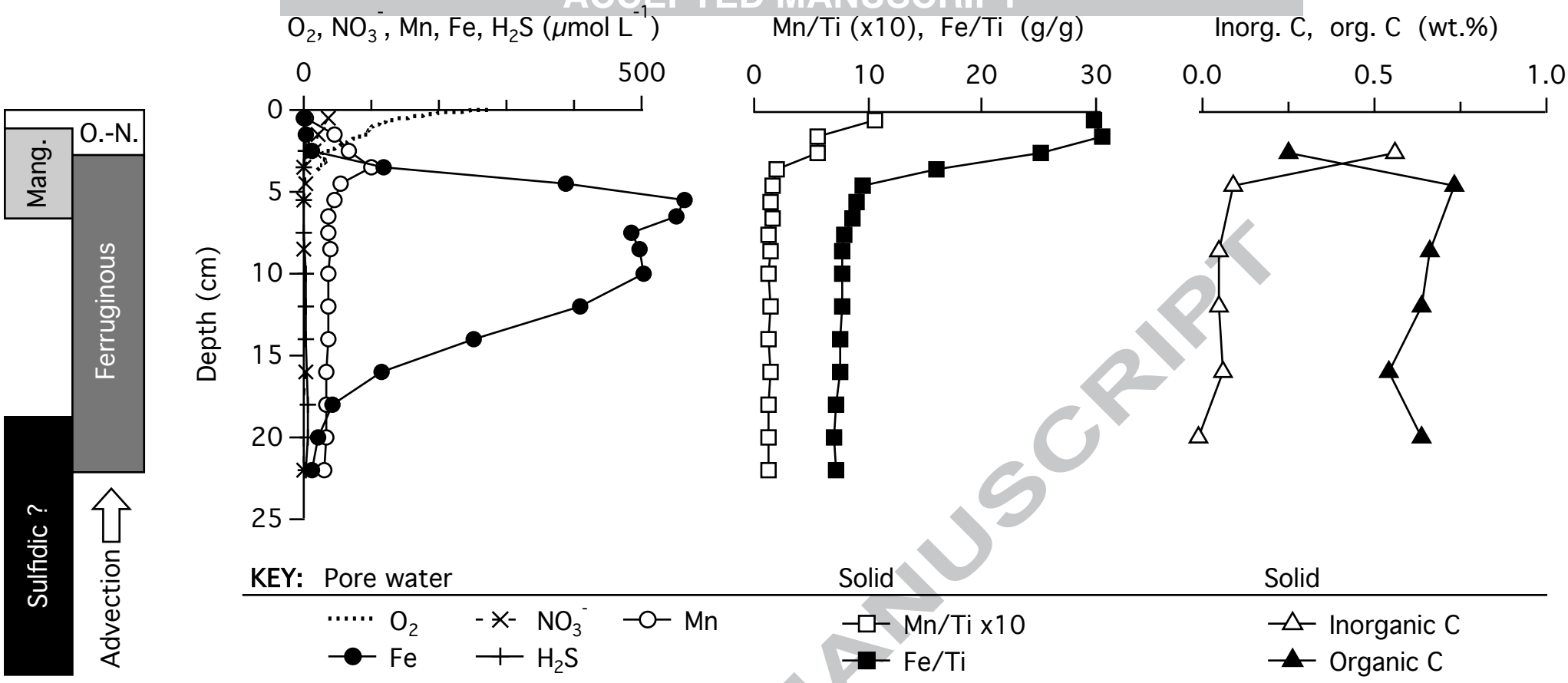

(b) MC7

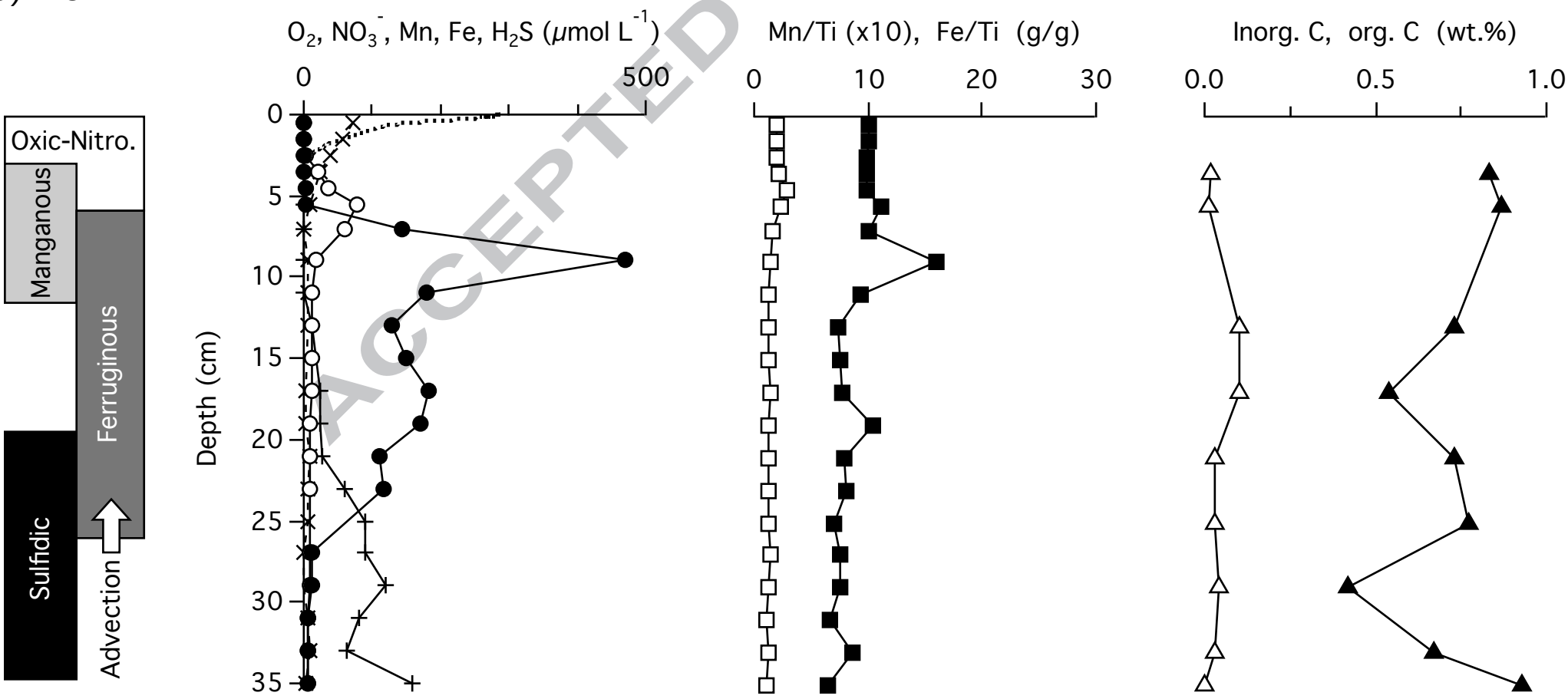

(c) MC1/2/3

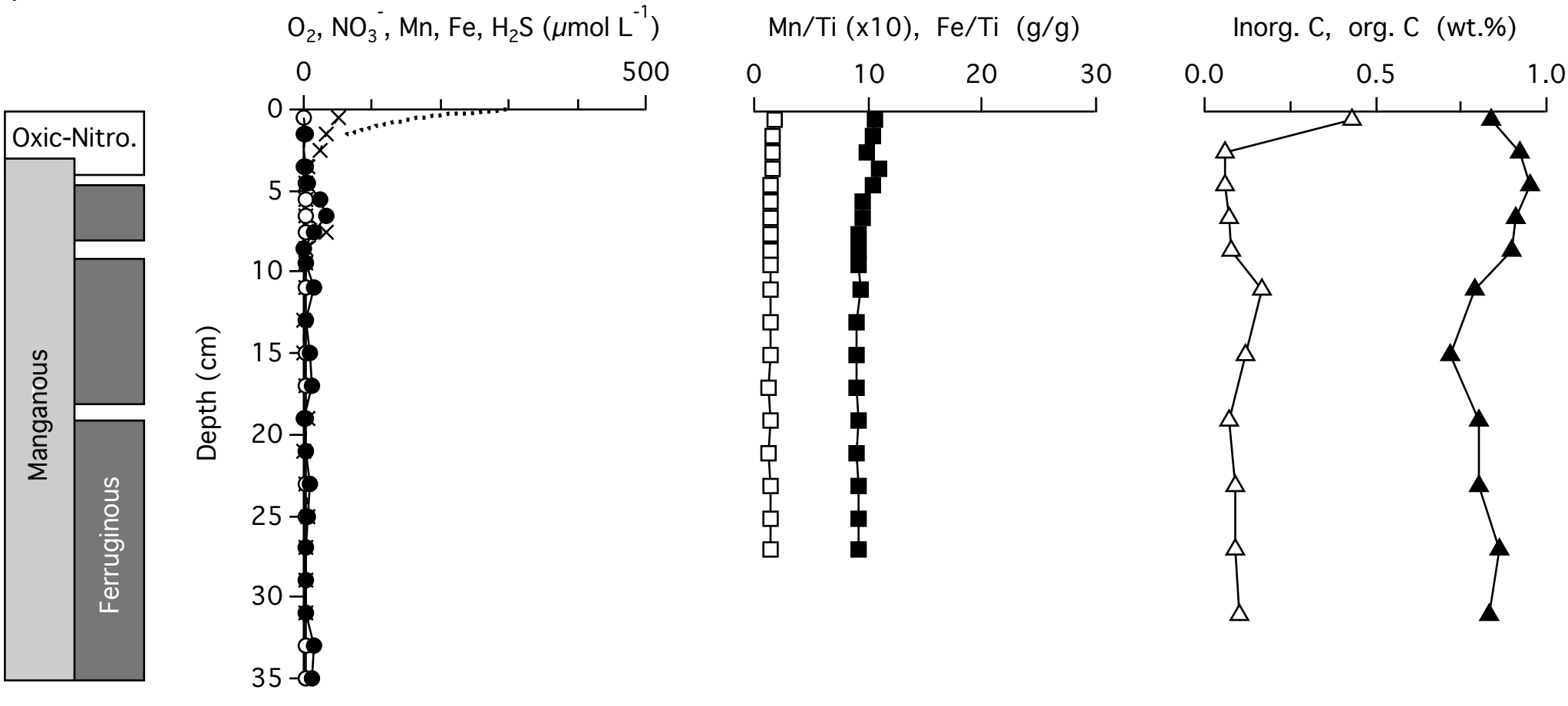

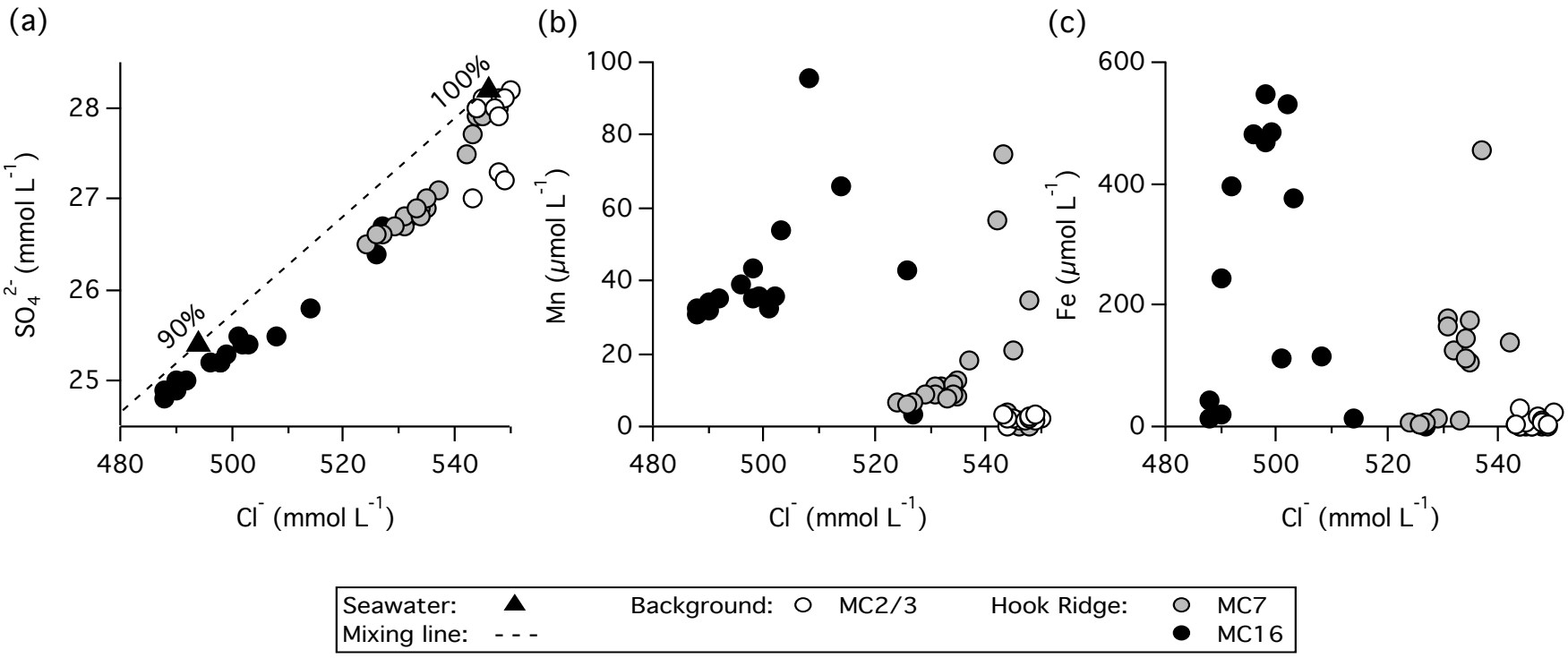

Aquilina et al., Fig. 3

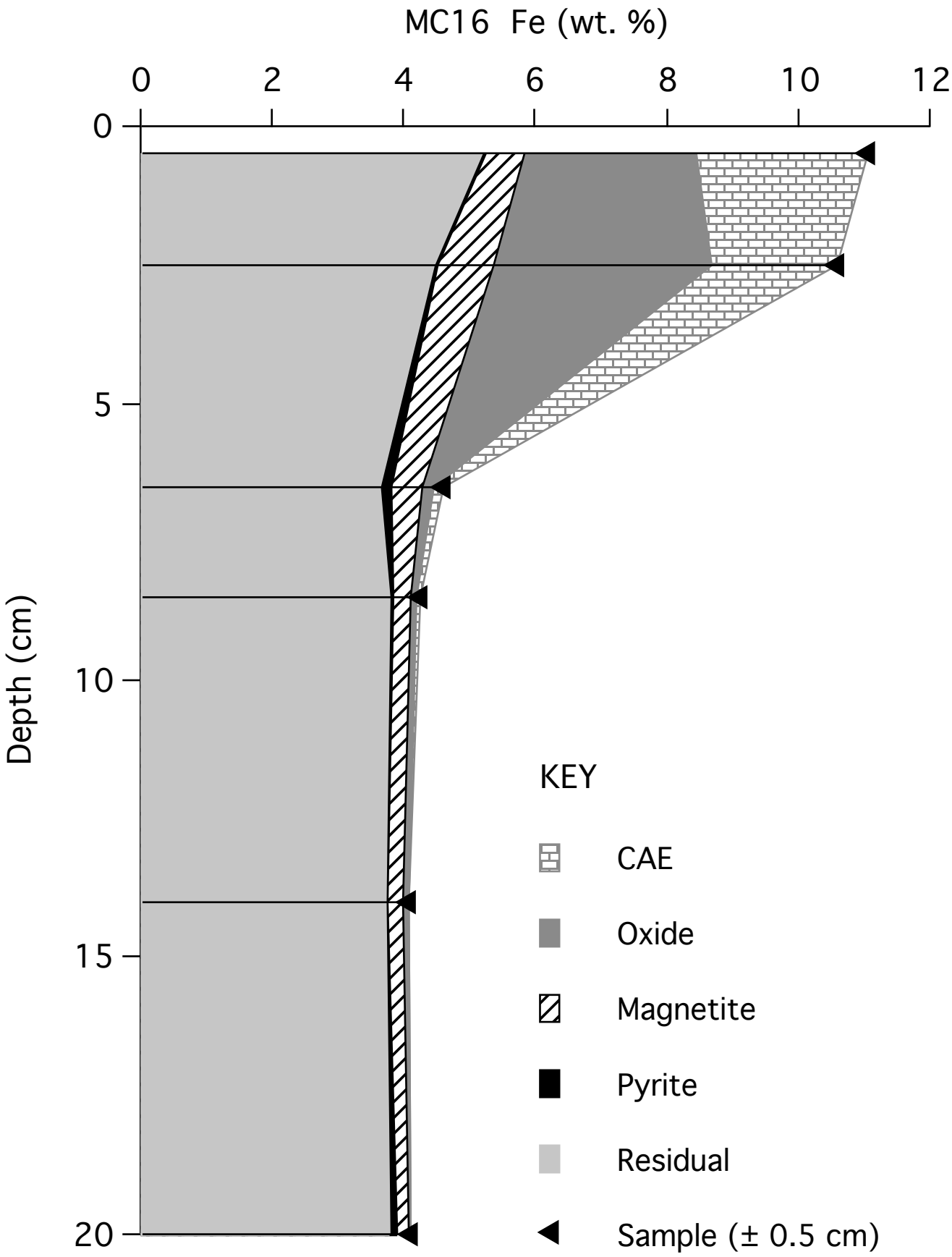

Aquilina et al., Fig. 4

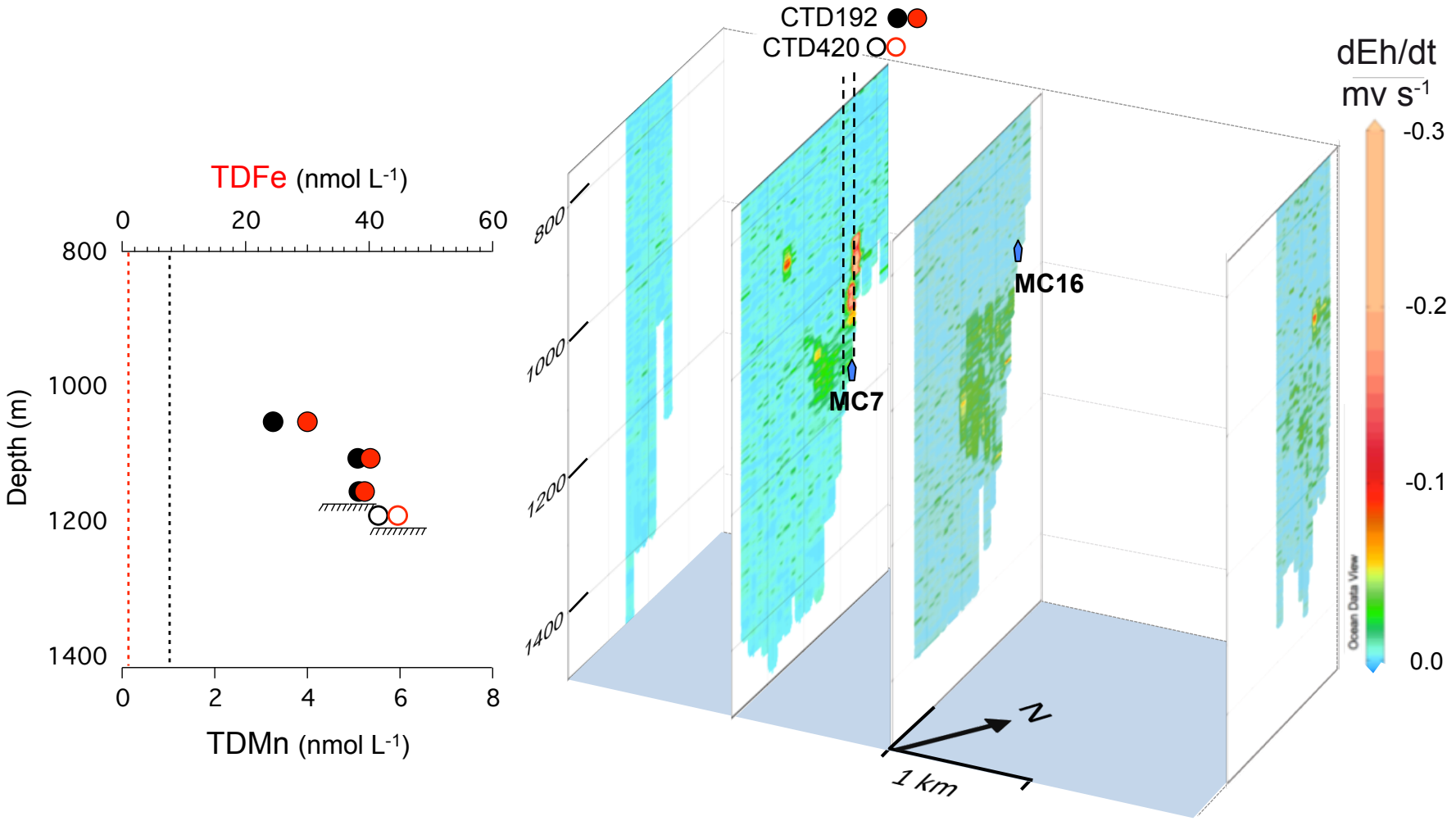

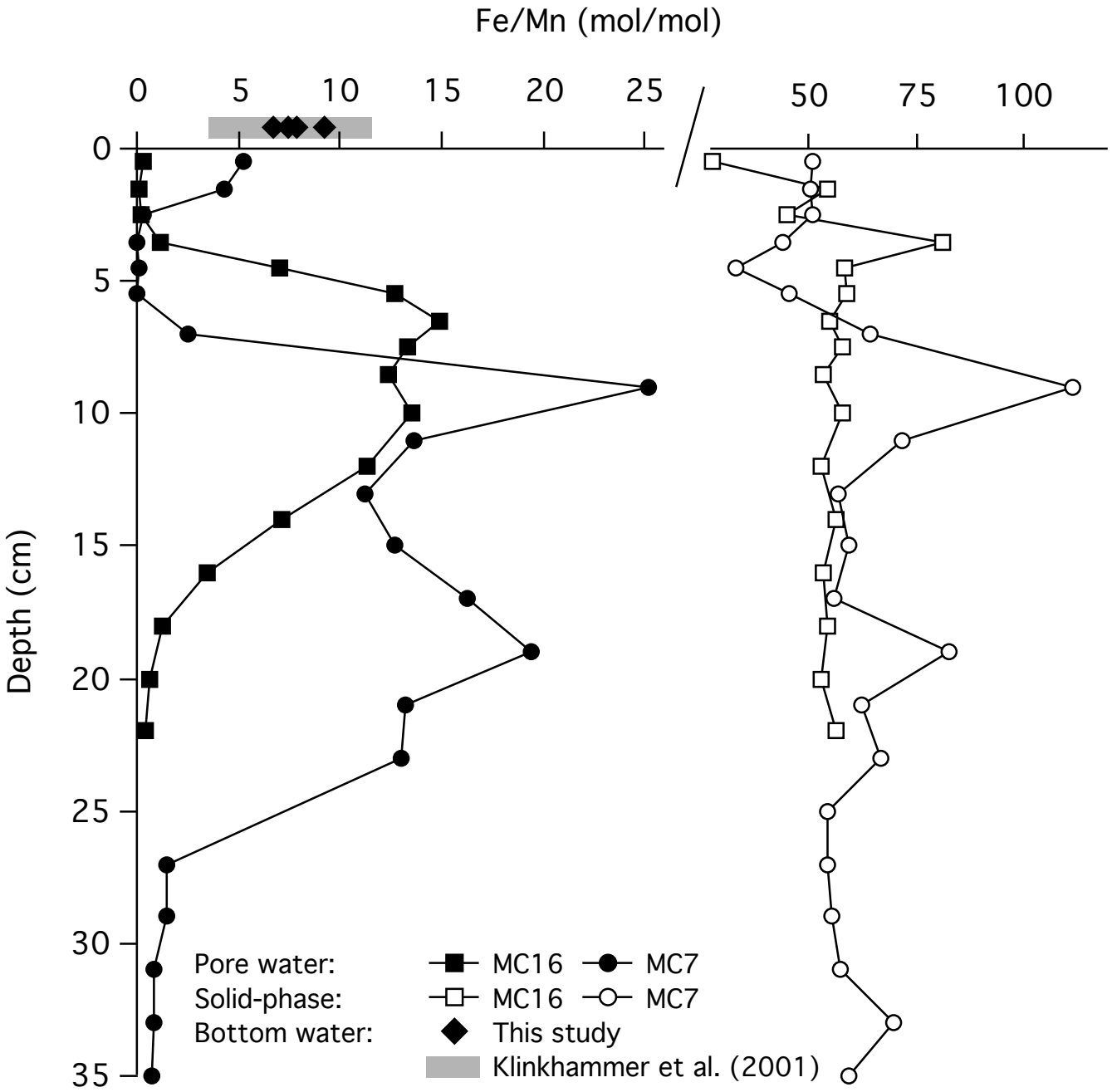

Aquilina et al., Fig. 6

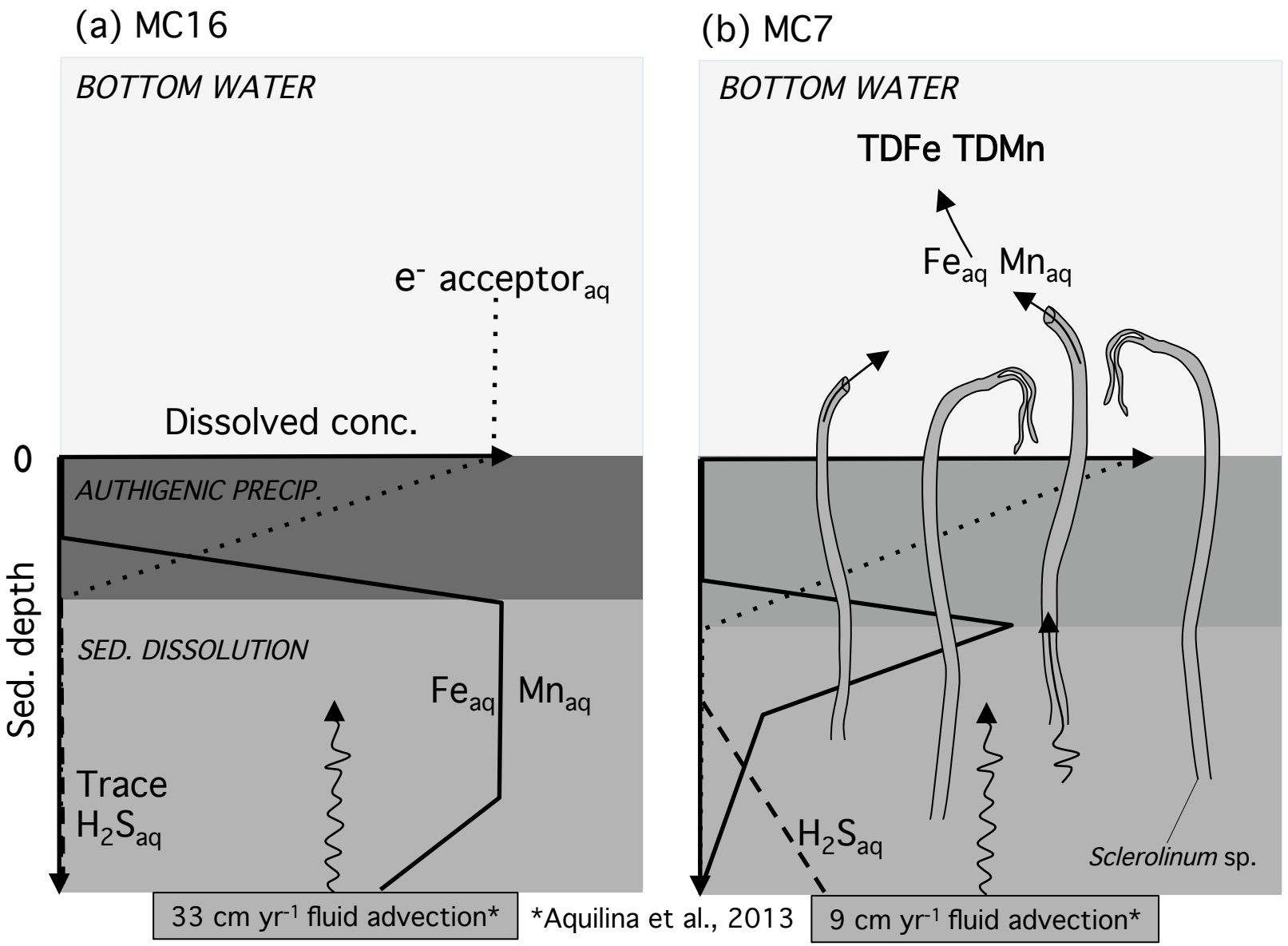

Aquilina et al., Fig. 7

Table 1. Measured abundance of Fe, Mn and Ti in Certified Reference Materials.

Cert. Ref. Material	Fe	Mn	Ti
Consensus values			
MAG-1	4.76 ± 0.42 wt. %	760 ± 69.0 ppm	4500 ± 420 ppm
GSMS-2	4.15 ± 0.11 wt.%	4570 ± 232 ppm	3660 ±180 ppm
NASS-5	3.70 ± 0.63 nmol L^{-1}	16.7 ± 1.04 nmol L^{-1}	-
Mean measured values[*]			
MAG-1; *n* = 3	4.85 ± 1.45 wt.%	764 ± 28.0 ppm	4220 ± 65.0 ppm
GSMS-2; *n* = 2	4.12 ± 0.28 wt.%	4580 ± 334 ppm	3460 ± 171 ppm
NASS-5; n = 7	3.74 ± 0.62 nmol L^{-1}	16.4 ± 1.60 nmol L^{-1}	-

- Not determined

[*]Mean of replicate number of samples (n), error quoted are ±1SD

Table 2. Pore water and solid-phase data collected from Bransfield Strait.

Site		Pore water							Solid-phase				
	Sed. depth	Cl^-	SO_4^{2-}	H_2S	O_2	NO_3^-	Fe	Mn	Fe	Mn	Ti	Inorg. C	Org. C
	cm	mmol L^{-1}	mmol L^{-1}	µmol L^{-1}	µmol L^{-1}	µmol L^{-1}	µmol L^{-1}	µmol L^{-1}	wt. %	wt. %	wt. %	wt. %	wt. %
Background													
MC1/2/3	0-1	544	28.0	-	185	51	bdl	bdl	4.92	0.08	0.47	0.43	0.84
MC1/2/3	1-2	-	28.8	-	68.1	33	4.02	0.06	4.82	0.08	0.46	-	-
MC1/2/3	2-3	-	28.3	-	-	22	bdl	bdl	5.02	0.08	0.51	0.06	0.92
MC1/2/3	3-4	546	28.1	-	-	5.2	bdl	1.47	4.85	0.07	0.44	-	-
MC1/2/3	4-5	545	28.1	-	-	2.8	6.97	2.44	4.69	0.06	0.45	0.06	0.95
MC1/2/3	5-6	550	28.2	-	-	2.3	23.2	2.07	4.39	0.06	0.46	-	-
MC1/2/3	6-7	544	28.0	-	-	2.0	31.8	2.31	4.55	0.07	0.48	0.07	0.91
MC1/2/3	7-8	-	-	-	-	*	16.3	1.65	4.13	0.06	0.45	-	-
MC1/2/3	8-9	549	28.1	-	-	2.3	bdl	1.42	4.24	0.07	0.46	0.08	0.90
MC1/2/3	9-10	-	-	-	-	2.1	3.36	1.46	4.23	0.06	0.46	-	-

MC1/2/3	10-12	547	28.0	-	-	3.0	15.5	1.59	4.43	0.07	0.48	0.17	0.79
MC1/2/3	12-14	-	-	-	-	1.0	2.49	1.73	4.31	0.06	0.48	-	-
MC1/2/3	14-16	548	27.9	-	-	1.0	10.3	2.09	4.43	0.07	0.50	0.12	0.72
MC1/2/3	16-18	-	-	-	-	1.5	12.7	2.22	4.15	0.06	0.46	-	-
MC1/2/3	18-20	554	28.0	-	-	6.0	bdl	2.32	4.49	0.07	0.49	0.07	0.80
MC1/2/3	20-22	551	27.8	-	-	0.7	3.76	2.61	4.18	0.06	0.46	-	-
MC1/2/3	22-24	584	27.7	-	-	2.4	7.51	2.84	4.16	0.06	0.45	0.09	0.80
MC1/2/3	24-26	548	27.3	-	-	4.8	5.47	3.00	4.15	0.06	0.45	-	-
MC1/2/3	26-28	543	27.0	-	-	1.6	4.15	3.22	3.94	0.06	0.43	0.09	0.86
MC1/2/3	28-30	549	27.2	-	-	3.7	2.56	3.28	-	-	-	-	-
MC1/2/3	30-32	-	28.3	-	-	3.5	3.73	2.91	-	-	-	0.10	0.83
MC1/2/3	32-33	-	-	-	-	-	15.2	3.00	-	-	-	-	-
MC1/2/3	33-36	-	-	-	-	-	11.7	3.45	-	-	-	-	-
Hook Ridge													
MC7	0-1	546	28.1	bdl	175	70	1.11	0.21	5.19	0.10	0.52	-	-

MC7	1-2	548	28.1	bdl	57.7	58	bdl	0.14	5.53	0.11	0.55	-	-
MC7	2-3	544	27.9	bdl	8.74	38	1.28	4.14	5.25	0.10	0.54	-	-
MC7	3-4	545	27.9	bdl	-	23	bdl	21.4	5.49	0.12	0.55	0.02	0.83
MC7	4-5	548	28.0	bdl	-	*	2.45	35.7	5.08	0.15	0.51	-	-
MC7	5-6	543	27.7	bdl	-	9.4	3.10	77.5	5.67	0.12	0.51	0.01	0.87
MC7	6-8	542	27.5	bdl	-	1.2	144	58.4	5.22	0.08	0.52	-	-
MC7	8-10	537	27.1	bdl	-	4.9	470	18.7	7.84	0.07	0.49	-	-
MC7	10-12	535	26.9	12	-	6.3	180	13.2	4.75	0.07	0.51	-	-
MC7	12-14	532	26.8	23	-	5.6	128	11.4	4.21	0.07	0.57	0.10	0.73
MC7	14-16	534	26.9	25	-	*	150	11.8	4.21	0.07	0.56	-	-
MC7	16-18	531	26.7	28	-	2.6	184	11.3	4.47	0.08	0.57	0.10	0.54
MC7	18-20	531	26.8	61	-	4.2	171	8.81	5.69	0.07	0.54	-	-
MC7	20-22	535	27.0	91	-	8.6	111	8.38	4.61	0.07	0.58	0.03	0.73
MC7	22-24	534	26.8	89	-	6.4	116	8.87	4.81	0.07	0.60	-	-
MC7	24-26	531	26.8	119	-	4.9	-	-	3.91	0.07	0.56	0.03	0.77

MC7	26-28	533	26.9	81	-	1.1	11.4	8.07	4.65	0.08	0.62	-	-
MC7	28-30	529	26.7	63	-	bdl	13.3	9.25	5.24	0.09	0.70	0.04	0.42
MC7	30-32	527	26.6	160	-	6.3	5.76	6.58	3.23	0.06	0.49	-	-
MC7	32-34	524	26.5	122	-	7.5	6.02	7.07	3.94	0.06	0.46	0.03	0.67
MC7	34-36	526	26.6	121	-	2.4	4.49	6.14	3.02	0.05	0.46	0.00	0.93
MC16	0-1	527	26.7	-	157	36	1.07	3.24	11.1	0.39	0.37	-	-
MC16	1-2	526	26.4	-	86	21	3.57	44.4	11.7	0.21	0.38	-	-
MC16	2-3	514	25.8	2	39	14	13.3	68.1	10.6	0.23	0.42	0.56	0.25
MC16	3-4	508	25.5	1	23	bdl	119	98.8	7.47	0.09	0.47	-	-
MC16	4-5	503	25.4	-	-	1.7	389	55.8	5.28	0.09	0.55	0.09	0.73
MC16	5-6	498	25.2	1	-	bdl	565	44.7	4.70	0.08	0.52	-	-
MC16	6-7	502	25.4	-	-	bdl	551	36.9	4.64	0.08	0.54	-	-
MC16	7-8	498	25.2	1	-	bdl	485	36.4	4.20	0.07	0.54	-	-
MC16	8-9	496	25.2	-	-	0.1	497	40.1	4.25	0.08	0.55	0.05	0.66
MC16	9-11	499	25.3	2	-	bdl	502	37.1	4.12	0.07	0.54	-	-

MC16	11-13	492	25.0	4	-	-	410	36.2	3.93	0.07	0.51	0.05	0.64
MC16	13-15	490	24.9	3	-	bdl	251	35.2	4.09	0.07	0.54	-	-
MC16	15-17	501	25.5	-	-	2.9	114	33.6	4.09	0.08	0.54	0.06	0.54
MC16	17-19	488	24.8	6	-	bdl	43.0	33.6	4.04	0.07	0.57	-	-
MC16	19-21	490	25.0	6	-	bdl	21.1	33.0	4.13	0.08	0.58	-0.01	0.64
MC16	21-23	488	24.9	3	-	0.5	13.5	31.8	4.11	0.07	0.58	-	-

All background site data collected from MC2, except for pore water O_2 (MC1), and Fe and Mn (MC3).

MC1 Latitude: 62.3842°S Longitude: 57.2440°W, 1150 m water depth

MC2 Latitude: 62.3842°S Longitude: 57.2444°W, 1150 m water depth

MC3 Latitude: 62.3842°S Longitude: 57.2441°W; 1148 m water depth

MC7 Latitude: 62.1969°S Longitude: 57.2975°W, 1174 m water depth

MC16 Latitdue: 62.1924°S Longitude: 57.2784°W, 1040 m water depth

bdl Below detection limit

- Not determined

*Data excluded - see methods section.

Table 3. Solid-phase Fe partitioning in Hook Ridge sediments (MC16).

Sed. depth	Fe_{CAE}	Fe_{OX}	Fe_{MAG}	Fe_{Py}	Fe_{RES}
cm	wt. %	wt. %	wt. %	wt. %	wt. %
0-1	2.59	2.60	0.61	0.04	5.27
2-3	1.91	3.32	0.83	0.06	4.53
6-7	0.16	0.17	0.46	0.19	3.65
8-9	0.04	0.10	0.28	0.04	3.79
13-15	0.00	0.08	0.23	0.05	3.72
19-21	0.00	0.04	0.19	0.11	3.79

Fe_{CAE} - Carbonate, adsorbed and exchangable

Fe_{OX} - Reducible oxides

Fe_{MAG} - Magnetite

Fe_{PY} - Pyrite

Fe_{RES} – Residual

Table 4. Water column concentrations of TDFe and TDMn above Hook Ridge.

Station	Lat.	Long.	Depth	Height a.s.f.	TDFe	TDMn	Fe/Mn
	°S	°W	m	m	nmol L^{-1}	nmol L^{-1}	mol/mol
192[a]	62.1186	57.1786	1156	10	39.23	5.12	7.66
192[a]	62.1186	57.1786	1107	59	40.2	5.08	7.92
192[a]	62.1186	57.1786	1053	113	29.98	3.26	9.2
420[a]	62.1194	57.1747	1191	17	41.54	5.94	6.99
39[b]	62.1159	57.1659	1045	-	66.6	5.58	11.93
39[b]	62.1159	57.1659	1038	-	42.6	11.33	3.76
39[b]	62.1159	57.1659	1038	-	49.6	5.27	9.41

a.s.f.: Above seafloor

- Not determined

[a]This study.

[b]Klinkhammer et al. (2001).

Table 5. Diffusive and advective flux estimates within Hook Ridge sediments.

	D_s Fe at 0°C	Fe	D_s Mn at 0°C	Mn
Diffusive flux	x 10^{-6} cm^2 s^{-1}	mmol m^{-2} d^{-1}	x 10^{-6} cm^2 s^{-1}	mmol m^{-2} d^{-1}
MC7	2.36	226	2.00	21.6
MC16	2.36	311	2.11	48.3
	v*	Fe	v*	Mn
Advective flux	cm yr^{-1}	mmol m^{-2} d^{-1}	cm yr^{-1}	mmol m^{-2} d^{-1}
MC7	9	96.1	9	15.4
MC16	33	424	33	74.2
Peclet number	Pe(Fe)	Pe(Mn)		
MC7	0.43	0.71		
MC16	1.4	1.5		

*from Aquilina et al. (2013)